AN ABSTRACT OF THE THESIS OF

Zhaoda Yao for the degree of Master of Science in Electrical and Computer Engineering presented on September 15, 2016.

Title: Multi-User Massive MIMO Channel Estimation Based on Kalman Filters.

Abstract approved:

_____

Mario E. Magaña

In wireless communication, channel state information (CSI) is essential for data detection. Fast fading coefficients estimation is important in order to acquire accurate CSI. Kalman filters (KF) are widely used for real time parameter estimation and can be used to estimate the fast fading coefficients of a mobile communication channel. Previous attempts at applying the KF to estimate fast fading coefficients of a massive multiple input multiple output (MIMO) channel assume that the channel autocorrelation is constant or varies weakly. Due to the fact that the carrier frequency of 5G massive MIMO systems reach tens of giga hertz, the channel autocorrelation could vary more acutely. The large number of antennas used in massive MIMO also increases the size of channel coefficients matrix. Therefore, some previous approaches based on nonlinear KF lead to high computational complexity. In order to improve system robustness of a nonlinear time varying channel and ease the

computational demand, a combined channel coefficient and autocorrelation estimator based on the KF is presented in this thesis. With the substantially improved receiver channel diversity provided by the massive MIMO system, a fairly accurate channel autocorrelation estimate can be achieved with linear estimator. Compared to previous non-linear estimators, the proposed method is more practical because the computational complexity is reduced substantially. It is shown through simulation that our combined channel coefficients and autocorrelation estimator can improve the mean square error (MSE) for all possible variations of channel autocorrelation.

©Copyright by Zhaoda Yao
September 15, 2016
All Rights Reserved

Multi-User Massive MIMO Channel Estimation Based on Kalman Filters

by
Zhaoda Yao

A THESIS

submitted to

Oregon State University

in partial fulfillment of
the requirements for the
degree of

Master of Science

Presented September 15, 2016
Commencement June 2017

Master of Science thesis of Zhaoda Yao presented on September 15, 2016

APPROVED:

Major Professor, representing Electrical and Computer Engineering

Director of the School of Electrical Engineering and Computer Science

Dean of the Graduate School

I understand that my thesis will become part of the permanent collection of Oregon State University libraries. My signature below authorizes release of my thesis to any reader upon request.

Zhaoda Yao, Author

ACKNOWLEDGEMENTS

I would like to thank my parents who provide me the opportunity to study in Oregon State University. Especially, I want to thank my mother. Without her love and support, I would not have come so far in my education.

I feel much indebted to many people who have instructed and helped me in the writing of this thesis. First of all I would like to express my deepest gratitude to my major adviser, Dr. Mario E. Magaña, a respectable, responsible and resourceful scholar, who has provided me with valuable guidance in every stage of the writing of this thesis. I could not have completed my thesis without his endless help. It is my honor to have worked under his guidance. Also, I want to thank Dr. Burton, from the English department, for her appreciated suggestions during the thesis writing workshop. Finally, I wish to extend my thanks to all the professors who have instructed me during my graduate study.

Last by not the least, I also own my sincere gratitude to all my friends who have accompany with me during my stay in Corvallis. Particularly I want to thank Yichuan Tian, for her treasured comments and appreciated help during the time of writing this thesis.

TABLE OF CONTENTS

Page

TABLE OF CONTENTS (CONTINUED)

Page

LIST OF FIGURES

Figure Page

LIST OF FIGURES (Continued)

Figure Page

LIST OF TABLES

Table Page

1 Introduction

1.1 Challenges of Wireless Communication Systems

The two major challenges in modern wireless communication systems are the wireless channel's variation in time and signal interference between users [1]. The designed wireless communication systems need to handle both problems to make wireless signal transmissions successful. Wireless communication engineers have developed several channel estimation methods to tackle the time variation issues and designed multiple access methods to have multiple users communicating simultaneously. However, challenges will appear continually along with the ever-increasing needs coming from the market.

Currently, the cellular phone data rate is expected to have a 25%-50% annual growth through 2030 and beyond [2]. Driven by this continuously increasing need, the upcoming 5^{th} generation wireless communication system (5G) is expected to have a much better performance than the 4^{th} generation wireless communication system (4G) system that we are using today. Massive multiple input multiple output (MIMO) system is a promising technology that will boost up the 5G's performance as a backbone. Extensive research has shown that the increasing number of antennas deployed in the base station will lead to better signal to noise ratio (SNR), higher data rate, more spectrum and power efficiency, etc. [3-6]. Nevertheless, massive MIMO's tremendous advantages come with the requirement of a lot higher computational complexity for

channel estimation due to the large number of antennas at the base station. Although it has been proved that the massive MIMO has substantial performance gains compared to the conventional MIMO, it suffers more severe limitations from pilot contamination than the conventional MIMO. More specifically, the pilot contamination is caused by inter-cell interference (ICI) due to the fact that all cells are assigned the same pilot sequences. It has been proved that the massive MIMO's uplink measurement noise will decrease with the increase of the number of base station antennas base on the fact that each received signal at different antenna port is independent [6]. However, if frequency reuse factor is 1, the received signal will interfered by the neighbor cells [7]. Therefore, it is important to develop methods which can track the time varying channel and mitigate the ICI. **Fig. 1** illustrates a multi cell massive MIMO system, which has M antennas at each base station and has multiple users in each cell. The center cell's uplink communication suffers from ICI from its neighboring cells.

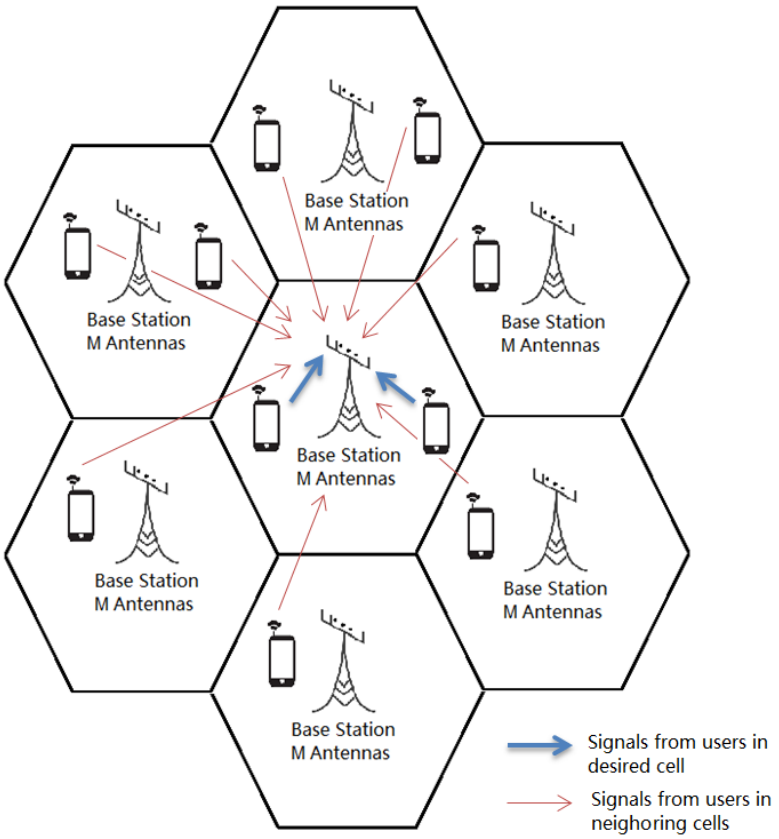

Figure 1.1 Illustration of massive MIMO system with ICI issue.

1.2 State of the Art of Massive MIMO

Scholars and researchers have conducted a lot of research to conquer the challenges mentioned previously. The uplink communication and downlink communication for a massive MIMO system is quite different because the base station side is assumed to have many more antennas than the mobile user side. To make channel estimation practical at the base station, time division duplexing (TDD) has been considered for the massive MIMO systems. Because the uplink and the downlink channels are reciprocal under TDD operation, TDD systems enable the channel estimation to be done at the base station, therefore easing the computational demand on the mobile devices [6].

However, some researchers have considered and continue to consider channel estimation at the mobile unit.

Masood [8, 9] proposed a collaborative channel estimation method at the base station side. She considered the measurements not only from each antenna but also from the neighboring antennas around the specific antenna. Laboratory results proved that her coordinated algorithm requires fewer pilot signals than traditional methods. For a frequency division duplexing (FDD) system, under the assumption of a compact square array with high correlation between channels, Lim and Chae [10] developed a compressive sensing based channel quantization feedback method that can reduce the channel estimation computational complexity at the mobile user side. In [11,12], Rao proposed a joint channel estimation scheme for FDD systems. The measurement is observed at the mobile user side while the channel estimation is done at base station side. He also developed two compressive sensing algorithms to reduce the pilot signal length. In [11], Rao proposed a modified orthogonal matching pursuit (OMP) that explores the joint sparsity in the channel matrix and converges much faster than the least squares (LS) method and other related strategies. Rao [12] later developed the modified subspace pursuit (MSP), which could further reduce the pilot signal length by introducing the prior support information from the channel history. In [13], Chen, and Yang proposed a method which decontaminates the measurements affected by pilot contamination. They use the difference between the desired channel and the contamination in power delay profile (PDP) to eliminate the contamination. To guarantee the performance of the decontamination method, they also suggested

a pilot assignment to randomize the interference. In [14], You proposed an adjustable phase shift pilot assignment to help the system have less pilot contamination. This new pilot assignment has a substantial spectral efficiency gain over the traditional orthogonal phase shift pilot under high mobility scenarios.

The above mentioned research tried to mitigate the pilot contamination problem by exploring the channel sparsity, channel spatial correlation and pilot efficiency in the wireless communication system. However, the channel coefficient may not always be constant in time. In reality, the wireless channel state information (CSI) is very important to system performance. In mobile scenarios, the coherence time varies inversely proportional to the Doppler spread. To make the communication process reliable, each frame should have duration shorter than coherence time. Namely, the time duration between two reference signals must be shorter than coherence time. A system with too small frame size will reduce its bit rate, which is definitely undesirable. Another approach is to have joint date detection and channel estimation methods, which can track the channel dynamically during one frame. A good channel tracker will ensure good system performance in a fast fading wireless communication environment even in the presence of pilot contamination. The channel estimation can be viewed as a state estimation problem [15]. Hence, we can consider the wireless channel as a dynamic system, where the channel coefficients are the states to be estimated. Kalman filter (KF) is a well-known real time estimation filter for linear dynamic system. The KF obtains the optimal minimum mean square state estimate for dynamic systems subject to

additive white Gaussian noise [15]. Therefore, the KF is an appropriate method for real-time channel coefficient estimation. The KF has already been studied and used by some researchers [16-20]. The channel dynamics can be approximated by a linear dynamic system if we assume the channel time correlation factor to be a constant. In [16], Sheikh proposed a KF based channel estimation method to track the coefficients of the time-selective fading channel in the multi-user single-input-multi-output systems. Karakaya [17] proposed an adaptive channel interpolator based on the KF to estimate the LTE uplink channel. The interpolator recovers the channel coefficients between two reference signals based on a linear channel assumption. However, the wireless channel does not vary linearly in a physical environment. Therefore, the assumption of a constant time correlation factor for the channel estimation is not accurate for practical systems. The authors in [18] developed a modified KF to estimate the channel coefficient and autocorrelation jointly. By considering the variation of the channel time correlation factor, authors in [19] developed algorithms based on KF to simultaneously estimate channel coefficients and time correlation factor. The authors of those two papers assumed the channel time correlation factor varies as a random walk system and developed the channel estimation algorithm for downlink and uplink channel estimation. Also, some researchers have used the KF for channel estimation in the frequency domain rather than in the time domain. As an example, the authors in [20] proposed a KF based channel estimator for orthogonal frequency division multiplexing (OFDM) systems that tracks the channel by tracking the signals' subspace. The KF works in the frequency

domain to recover the channel coefficients by subcarriers that carry only pilot signals. The system considered in [20] is not part of the current standard and has some pilot redundancy on its ‘pilot only’ carriers.

1.3 Proposed Method

In reality, wireless channels’ dynamics are not linear. The time correlation factor for the channel is can be modeled as a Bessel function of the first kind of zero order [21] and this factor changes nonlinearly with respect to the sampling time and the Doppler frequency spread.

5G systems focus on faster data rate and are based on a wider channel bandwidth assumption. Moreover, frequency bands far beyond 4.2GHz, which is currently using by 4G systems, are being considered. Recently, the FCC licensed more frequency spectrum for flexible use in 28GHZ, 37GHz, 39GHz, 40GHz and 69GHz [22]. A higher carrier frequency will lead to larger Doppler spread which will make 5G systems more likely to encounter a fast fading channel, and the channel time correlation factor will be more sensitive to the motion between transmitting and receiving antennas. Especially, when the mobile station is moving with high acceleration, the channel will be varying with a changing time correlation factor. On the one hand, the 5G with massive MIMO technology will substantially increase the channel diversity. On the other hand, it will increase channel estimation computational complexity. In this thesis, we propose a channel estimation method based on the Kalman filter, which can jointly estimate the channel time correlation factor and the channel coefficients for uplink transmission of 5G wireless communication systems.

The proposed method uses the channel diversity created by the massive receiving antenna array to mitigate the computational complexity caused by the increased number of antennas.

2 Background and Assumptions

2.1 Brief History of Wireless Communication

One of the most significant changes of human's life is the freedom of information exchange. After the first telephony system built in the early part of twenty century, people were able to eventually communicate with each other in spite of distance. After that, the telephone became an integral part of our daily life. However, our connection with the information's world was still limited by the wires.

The wireless communication system was first introduced in 1915 and grew slowly at the beginning. The pioneer wireless engineers designed wireless systems that had a central transmitter to serve a whole metropolitan area. Due to the inefficient use of frequency spectrum and the limitation of devices, the New York public wireless communication system could only support fewer than five hundred users in 1946 [23]. Though the wireless communication service was generally poor at that time, the potential of the market was very huge.

The cellular concept, which had been developed by researchers at AT&T Bell Laboratories, was a brilliant idea to expand the capacity. Because the power of a wireless signal decays exponentially with the distance, the cellular system spatially separate users in a big area into different sections. This design allows multiple users access to different base stations simultaneously using same operating frequency. Also, the total transmission power could be reduced

significantly. The first analog cellular system was deployed in 1983 in Chicago which became saturated by 1984. Beyond almost everyone's expectation, the explosive growth of wireless communications had begun [24]. **Fig. 2.1** illustrates the basic spatial structure of a cellular system.

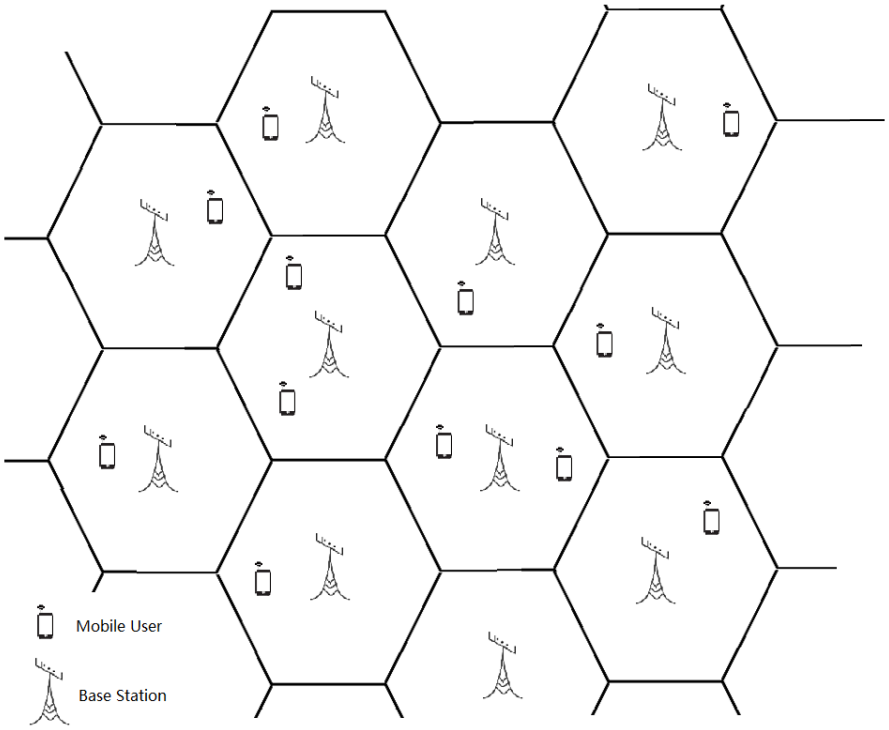

Figure 2.1 Cellular system structure.

Driven by the need of higher capacity, faster speed, better quality, better power efficiency, etc., the second generation cellular systems changed from analog to digital. Second generation cellular systems only offered voice service at the very beginning. Then, with the development and popularity of the internet, those systems evolved to progressively offer data service in order to meet the emerging demand of internet services [23]. Since then, the structures of the cellular systems were basically developed similar to the current structure.

Currently, in cellular systems, the voice service has become a small portion compared to the enormous internet data stream cost by manifold smart phones' applications. The need of higher data throughput rate is growing with the rapid evolution of smart phone technologies. Therefore, it is reasonable that in the ensuing generations of cellular systems, namely 3G and 4G, the changes in standards are mainly aimed at accelerating the data rate and to achieve better spectrum efficiency.

2.2 Wireless Fading Channel

2.2.1 Channel Fading

The wireless channel coefficients are directly determined by the geographical characteristic of the cellular system. In baseband form, a wireless point to point channel can be described by [25]

$$g(t) = h(t) \cdot \beta(t), \tag{2.1}$$

where the channel $g(t)$ is comprised of the small scale fading coefficient $h(t)$ and the large scale fading coefficient $\beta(t)$. **Fig. 2.2** shows the fading effect in terms of signal power versus the transmission distance.

The large scale fading, which is also called shadow fading, is due to the terrain contours between the transmitter and receiver [23]. The shadow fading can be treated as a quasi-static value due to its slow variation. Usually, we can use power control to partially compensate for the shadow fading. In this thesis, we treat it as a known constant. The most popular statistical model for shadow

fading is the slope-intercept models [26] that will be discussed in next chapter.

The small scale fading, which is also called multipath fading, is a relatively fast changing value in the wireless system. The statistical model and the dynamics of multipath fading will be discussed in later sections. **Fig. 2.2** illustrates the small scale and the large scale fading.

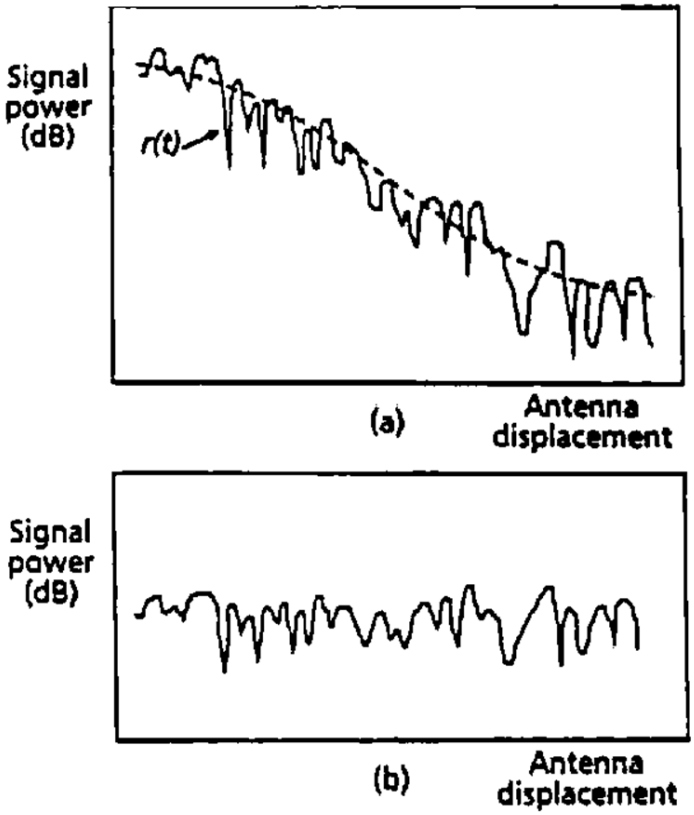

Figure 2.2 Illustration of large scale fading and small scale fading [26].

Fig. 2.2 illustrates the phenomenon that signal power attenuates with distance. The dotted line in **Fig. 2.2 (a)** represents the large scale fading and **Fig. 2.2 (b)** shows the corresponding multipath fading [26].

2.2.2 Multipath Phenomena

Electromagnetic waves are reflected, refracted, scattered, transmitted, diffracted and absorbed by objects that appear on their propagation path. **Fig. 2.3** illustrates the effects that could happen during the radio signals' propagation.

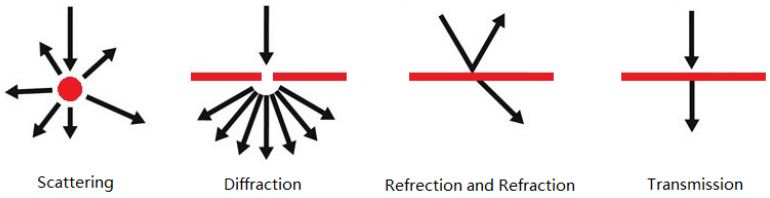

Figure 2.3 Physical effects of electromagnetic wave propagation.

For a transmitter side equipped with non-directional antenna, the transmitted signal will travel many different paths to reach the receiver side. **Fig. 2.4** illustrates the multipath phenomena of a system's uplink communication in an urban area.

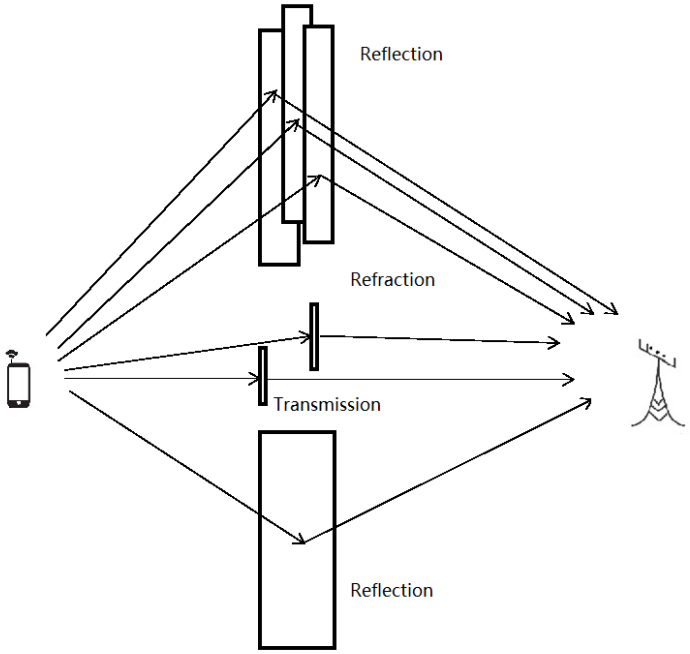

Figure 2.4 Urban area multipath phenomenon.

Multipath phenomenon could contribute to the receiver side either constructively or destructively. Arriving signals randomly add up or cancel out depend on their random phase shifts. This effect is called multipath fading or small scale fading. The multipath fading can be classified into discrete multipath fading and diffuse multipath fading [26]. The discrete multipath fading channel is made up of a small and identifiable number of paths that are created by small hills or buildings. The number of multipath channel components is finite. The diffuse multipath fading channel is made up of a large number of unresolvable multipath components. This kind of multipath fading environment mostly appears in urban areas where the space between mobile user and base station is filled up with objects such as buildings and plants [26].

Often, in an urban area, there might be no line of sight (LOS) path between the transmitting antennas and the receiving antennas. In other words, the environment causes rich scattering of signals. The associated channel is called a Rayleigh fading channel. Otherwise, if a LOS path exists between each side, the channel is called a Ricean fading channel.

2.2.3 Multipath Channels Baseband Equivalent Description

Signals traveled through different paths will contribute to the receiver as superposition. Therefore, the receiver side will receive overlaid replicas of the original transmitted signal. Due to the different length and different electromagnetic property of each path, the received replicas will have different attenuation factors and time delays. **Eq. 2.2** represents a signal observed at the receiver side.

$$r(t) = \sum_n a_n(t) s_m(t - \tau_n(t)), \tag{2.2}$$

where $r(t)$ is the received signal, $s_m(t)$ is the transmitted modulated signal, $a_n(t)$ is the attenuation factor of the signal that traveled through the n^{th} path and $\tau_n(t)$ is the time delay of signal traveled through the n^{th} path.

Signals are comprised of real and imaginary components. We can further express received signal $r(t)$ as

$$r(t) = \sum_n a_n(t) s_{mI}(t - \tau_n(t)) + \sum_n a_n(t) s_{mQ}(t - \tau_n(t)), \tag{2.3}$$

where

$$s_{mI}(t - \tau_n(t)) = s_I(t - \tau_n(t)) \cos[(\omega_c + \omega_n)(t - \tau_n(t))],$$

$$s_{mQ}(t - \tau_n(t)) = s_Q(t - \tau_n(t)) \sin[(\omega_c + \omega_n)(t - \tau_n(t))],$$

$s_{mI}(t)$ and $s_{mQ}(t)$ are the in-phase components and quadrature components of the modulated signal respectively, and $s_I(t)$ and $s_Q(t)$ are the in-phase component and quadrature component of the transmitted base band signal, respectively.

Also, when user mobility occurs, the signal is affected by the Doppler shift,

$$f_D = \frac{v}{c} f_c, \tag{2.4}$$

where v is the mobile user speed, f_c is the carrier frequency and c is the speed of light. The Doppler shift is physically due to the relative motion between transmitter and the receiver.

We can further express the received baseband signal as

$$r_b(t) = r_{bI}(t) + j\, r_{bQ}(t), \tag{2.5}$$

where

$$r_{bI}(t) = \sum_n a_n(t)\, s_I(t - \tau_n(t)) \cos(2\pi f_c \tau_n(t) - 2\pi f_D(t - \tau_n(t)),$$

and

$$r_{bQ}(t) = \sum_n a_n(t)\, s_Q\big(t - \tau_n(t)\big)\sin(2\pi f_c \tau_n(t) - 2\pi f_D\big(t - \tau_n(t)\big).$$

Let

$$\varphi_n(t) = 2\pi f_c \tau_n(t) - 2\pi f_D(t - \tau_n(t)), \tag{2.6}$$

then the baseband channel can be expressed as

$$c(t) = \sum_n \delta\big(t - \tau_n(t)\big) a_n(t) e^{-\varphi_n(t)}, \tag{2.7}$$

where the in-phase and the quadrature components are

$$c_I(t) = \sum_n \delta(t - \tau_n(t)) a_n(t)\cos(\varphi_n(t)),$$

$$c_Q(t) = \sum_n \delta(t - \tau_n(t)) a_n(t)\sin(\varphi_n(t)).$$

2.2.4 Rayleigh Fading Channel

Since the objects on the paths of the signal are irregular, the received multipath signals have been reflected and scattered a large number of times in their path. By the central limit theorem, the amplitude attenuation factor $a_n(t)$ can be modeled as a Gaussian process. $\varphi_n(t)$ is the phase delay which is defined in **Eq. 2.5**. The carrier frequency f_c is assumed to be very large, therefore any small change in $\tau_n(t)$ can cause the phase to rotate over 2π. Hence, the phase-shift $\varphi_n(t)$ is uniformly distributed between $[0, 2\pi]$. Then, each multipath channel coefficient $a_n(t)e^{-\varphi_n(t)}$ can be modeled as a complex

Gaussian process. A complex Gaussian distribution is a joint Gaussian distribution with two detentions comprised of the real axis and imaginary axis. Because the phase delay is a uniform random variable, the two dimensions of the complex Gaussian process is uncorrelated and therefore independent. **Fig. 2.5** illustrated the independent complex Gaussian distribution. a_n is the attenuation factor and $\tau_n(t)$ is the phase delay.

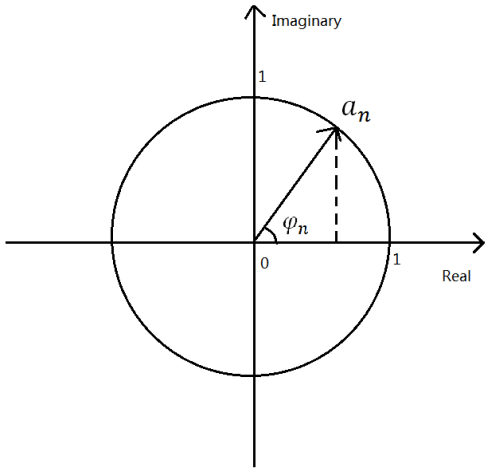

Figure 2.5 Illustration of the amplitude factor and the phase angle.

For a narrow band signal whose symbol time is much larger than the delay spread, the **Eq. 2.7** can be rewritten as,

$$C_I(t) = \sum_n a_n(t)\cos\left(\varphi_n(t)\right),$$

$$C_Q(t) = \sum_n a_n(t)\sin\left(\varphi_n(t)\right),$$

$$c(t) = \sum_n a_n(t)e^{-\varphi_n(t)}. \qquad (2.8)$$

In this thesis, we consider 5G systems deployed in an urban area in which it is

reasonable to assume the signals are richly scattered. So, there will be no LOS path appearing in the multipath channel. And it further implies that there is no dominant $a_n(t)$ in the channel. If the signals are rich scattered, the number of paths is also large and the channel can be considered as a diffuse multipath fading channel. Then the channel coefficient is approximated to be a zero mean complex Gaussian random variable whose two dimensions are independent. Then, the envelop of this coefficient is therefore a Rayleigh random variable. Such channel is called a Rayleigh fading channel.

2.2.5 Dynamics of channel

The wireless channel multipath fading coefficients almost never stop changing due to the motion of mobile users. In order to design a real time wireless channel estimator, it is necessary to model the wireless channel's dynamics mathematically. First, the expectation of the in phase and quadrature channel components are,

$$E[c_I(t)] = E\left[\sum_n a_n(t)\cos\left(\varphi_n(t)\right)\right] = \sum_n E[a_n(t)]\ E[\cos\left(\varphi_n(t)\right)] = 0, \quad (2.9)$$

$$E[c_Q(t)] = E\left[\sum_n a_n(t)\sin\left(\varphi_n(t)\right)\right] = \sum_n E[a_n(t)]\ E[\sin\left(\varphi_n(t)\right)] = 0. \quad (2.10)$$

The cross correlation between the in phase part and the quadrature part is

$$E[c_I(t)c_Q(t)] = E\left[\sum_n a_n(t)\cos\left(\varphi_n(t)\right)\sum_m a_m(t)\sin\left(\varphi_m(t)\right)\right]. \quad (2.11)$$

Since the paths are independent to each other,

$$E[c_I(t)c_Q(t)] = \sum_n E[a_n^2(t)]E\left[\cos\left(\varphi_n(t)\right)\sin\left(\varphi_n(t)\right)\right] = 0. \quad (2.12)$$

Thus the in phase and the quadrature part are uncorrelated, and they are also independent due to the property of Gaussian process.

During a short time slot, the attenuation factor and the time delay are assumed to be constant. Therefore the phase shift angle $\varphi_n(t)$ is also a constant. Then, under the wide sense stationary uncorrelated scattering (WSS) assumption, the time correlation for in phase channel can be derived as,

$$E[c_I(t)c_I(t+\Delta t)] = \sum_n E[a_n^2]E\left[\cos\left(\varphi_n(t)\right)\cos\left(\varphi_n(t+\Delta t)\right)\right]. \quad (2.13)$$

Substituting **Eq. (2.5)** into **Eq. (2.12)**, yields

$$E[c_I(t)c_I(t+\Delta t)] = \sum_n E[a_n^2]E\left[\frac{1}{2}\cos(2\pi f_D\Delta t) - \frac{1}{2}\cos(2\varphi_n - 2\pi f_D\Delta t)\right]. \quad (2.14)$$

Because f_c is very large, therefore $2\varphi_n$ is large enough such that $2\pi f_D\Delta t$ can be ignored. The significantly large φ_n will lead to a uniformly random distributed phase angle within $[0, 2\pi]$. Then, the **Eq. 2.13** can be rewritten as

$$E[c_I(t)c_I(t+\Delta t)] = \frac{1}{2}\sum_n E[a_n^2]E[\cos(2\pi f_D\Delta t)]. \quad (2.15)$$

Assume the angle between the n^{th} path and the mobile user's moving direction is θ_n, which is illustrated in **Fig. 2.6**.

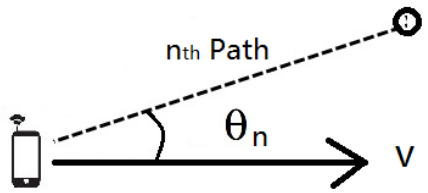

Figure 2.6 Included angle between moving direction and nth path.

Then, the **Eq. (2.14)** can be further expressed as

$$E[c_I(t)c_I(t+\Delta t)] = \frac{1}{2}\sum_n E[a_n^2]E\left[\cos\left(\Delta t\, 2\pi f_c \frac{v}{c}\cos\theta\right)\right]. \quad (2.16)$$

Clarke in [21] and Jakes in [27] introduced the uniform scattering environment which is common in an urban area. For such a model which is showed in **Fig. 2.7**, the multipath signals come from all the direction to the mobile device and a mobile device with non-directional antenna will radiate its signals to all directions.

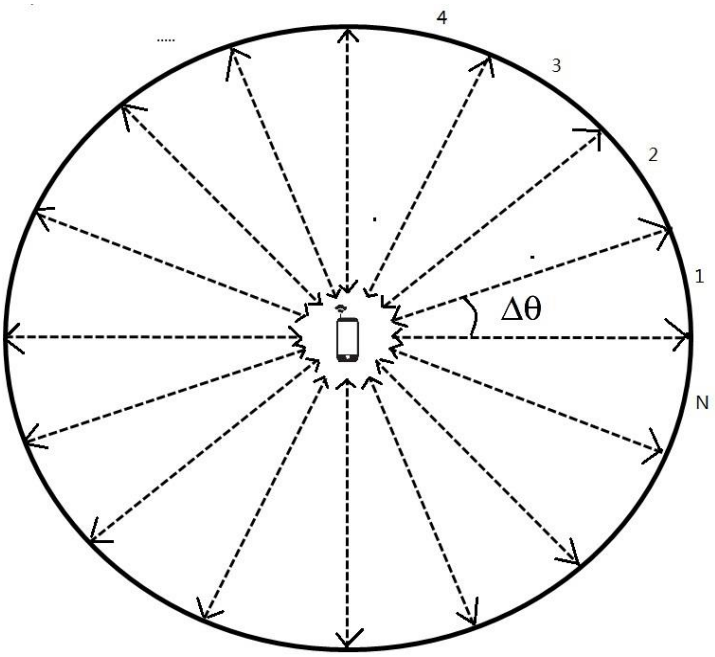

Figure 2.7 One ring model for rich scattering environment.

Assuming each direction has same signal power and the total power is P, we get

$$E[c_I(t)c_I(t+\Delta t)] = \frac{P}{2N}\sum_n \cos\left(\Delta t\, 2\pi f_c \frac{v}{c}\cos\theta_n\right), \qquad (2.17)$$

where

$$N = \frac{2\pi}{\Delta\theta}.$$

If the number of multipath components approaching infinite and the included angles $\Delta\theta$ are identically approaching zero, the time correlation of channel will become,

$$E[c_I(t)c_I(t+\Delta t)] = \frac{P}{4\pi}\int_0^{2\pi} \cos\left(\Delta t\, 2\pi f_c \frac{v}{c}\cos\theta\right) d\theta. \qquad (2.18)$$

The time correlation of the quadrature channel is similar to **Eq. (2.18)**,

$$E[c_Q(t)c_Q(t+\Delta t)] = \frac{P}{4\pi}\int_0^{2\pi} \sin\left(\Delta t\, 2\pi f_c \frac{v}{c}\cos\theta\right) d\theta, \qquad (2.19)$$

Thus the complex channel time correlation is expressed as,

$$a(\Delta t) = E[(c_I(t) + j\, c_Q(t))(c_I(t+\Delta t) + jc_Q(t+\Delta t))],$$

$$a(\Delta t) = \frac{P}{2\pi}\int_0^{2\pi} \cos\left(\Delta t\, 2\pi f_c \frac{v}{c}\cos\theta\right) d\theta$$

$$= \frac{P}{2\pi}\int_0^{2\pi} \frac{e^{j\Delta t\, 2\pi f_c \frac{v}{c}\cos\theta} + e^{-j\Delta t\, 2\pi f_c \frac{v}{c}\cos\theta}}{2} d\theta$$

$$= \frac{P}{\pi}\int_0^{\pi} e^{j\Delta t\, 2\pi f_c \frac{v}{c}\cos\theta}\, d\theta$$

$$= P\, J_0(2\pi f_D \Delta t), \qquad (2.20)$$

where

$$J_0(x) = \frac{1}{\pi}\int_0^{\pi} e^{-jx\cos\theta}\, d\theta \ ,$$

is the Bessel function of the first kind of 0^{th} order [28].

2.3Massive Multiple Input Multiple Output Systems Uplink Communication

2.3.1 Massive MU-MIMO Systems

Massive MIMO systems are referred to systems which operate with a large number of antennas at both transmitter and receiver. The massive MIMO system substantially improves the channel diversity gain and the channel

multiplexing gain. However, there is a fundamental tradeoff between the channel diversity gain and the channel multiplexing gain, which is well discussed in [29]. The channel diversity gain will directly help the systems to have a better SNR, and the channel multiplexing gain enables the spatial division multiple access (SDMA) to accomplish better spectral efficiency. The massive MIMO systems also promise to be more power efficient, which is mainly due to the base stations use beam forming technique at the transmission period that lowers the operation voltage [25].

The wireless channel results in a received signal which is a combination of all the transmitted signals. **Eq. (2.20)** expresses the relationship between the transmitted and received signals.

$$\mathbf{y}(t) = \sqrt{Pt}\mathbf{G}(t)\mathbf{x}(t) + \mathbf{w_c}(t), \qquad (2.21)$$

where $\mathbf{y}(t)$ is the received signal vector, $\mathbf{x}(t)$is the transmitted signals vector, Pt is the transmitted signals power, $\mathbf{G}(t)$ is the channel coefficients matrix and $\mathbf{w_c}(t)$ represents the combination of noise and interference. For a multiple massive MIMO (MU-MIMO) system which all mobile users have only one antenna, every element in the signal vector $\mathbf{x}(t)$ is from different user. If the antennas are deployed with distance more than half wavelength, the channel of different data stream is approximately independent [23]. If we assume all mobile users are randomly located in each cell and the antennas at the base station are carefully deployed, the elements in channel coefficient matrix $\mathbf{G}(t)$ will be independent of each other. Thus, the degree of freedom of the received signal is proportional to the transmitter antennas and the channel diversity is

proportional to the number of receiver antennas. The SDMA and Massive MIMO systems' channel diversity combining will be discussed in the following sections.

2.3.2 Spatial Division Multiple Access

Unlike a wired communication channel, the wireless communication channel uses the 'air' as its medium, and therefore all the users are basically connected together. For practical mobile systems, the separation of different users' data stream is important. Numerous methods have been proposed to find an optimal way to have as many users as possible connected and provide desired data rate for every user. Unlike frequency division multiple access (FDMA) or time division multiple access (TDMA), SDMA is considered to be a more efficient scheme for the 5G wireless communication systems. The relationship between the received signals and the transmitted signals in the uplink communication is described by **Eq. (2.21)**. In the uplink communication, the receiver side can recover the overlaid signals using receiver algorithms such as zero forcing (ZF), successive interference cancellation (SIC) and maxim likelihood (ML). For the systems that have similar number of antennas at transmitter and receiver side, the ZF algorithm will not perform well, due to the pseudo inverse in the algorithm will also amplify the noise while recovering the received signal. Thus, ML algorithm and some ML approximation algorithms can be used to improve the performance of data detection. Though the ML algorithm provides the optimal detection performance, the computational complexity is very high. It grows exponentially with the number of mobile users and the modulation

level. SIC is an iterative algorithm that detects each data stream successively in order to avoid amplify the received noise. It is a compromise between performance and the computational complexity. For a MU-MIMO system where the number of antennas at the base station is assumed to be much more than the number of mobile user, the performance of ZF will be improved significantly due to the substantially increased channel diversity gain.

2.3.3 Wireless Channel Diversity

Deep channel fading is due to the randomness of the physics of the mobile channel which causes a large power penalty and harms the system performance. Diversity combining is an effective method to mitigate deep channel fading, which uses the fact that the probability of multiple independent fading paths experiencing deep channel fading simultaneously is very low [23]. Massive MIMO systems have a large number of antennas at base station, which makes the received signals have large receiver diversity, enabling effective diversity combining.

Selection diversity combining (SDC), equal gain combining (EGC) and maximum ratio combining (MRC) are well known detection strategies for multiple receiver diversity combining. With accurately estimated channel coefficients, SDC chooses the received signal from the channel with best SNR and rotates the signal by the angle of the channel. EGC directly rotates the entire received signal with their corresponding channel angles and then sums them up with equal weight. MRC is similar to EGC except it weights each channel by their channel amplitude. **Eq. (2.22)** shows the MRC algorithm,

$$\mathbf{D}(t) = \sqrt{Pt}\mathbf{G}^*(t)\mathbf{y}(t), \tag{2.22}$$

where $\mathbf{G}^*(t)$ is the conjugate transpose of the channel coefficients matrix. The **Eq. (2.22)** can be further expanded as,

$$\mathbf{D}(t) = \sqrt{Pt}\mathbf{G}^*(t)\mathbf{G}(t)\mathbf{x}(t) + \mathbf{G}^*(t)\mathbf{n}(t). \tag{2.23}$$

Dividing both sides by the number of received antennas M, yields

$$\frac{1}{M}\mathbf{D}(t) = \frac{1}{M}\sqrt{Pt}\mathbf{G}^*(t)\mathbf{G}(t)\mathbf{x}(t) + \frac{1}{M}\mathbf{G}^*(t)\mathbf{n}(t), \tag{2.24}$$

The $\frac{1}{M}\mathbf{G}^*(t)\mathbf{G}(t)$ in **Eq. (2.23)** can be viewed as the autocorrelation of the channel coefficients matrix. Due to the independency of each channel, the correlation matrix approaches to an identity matrix when the M approaches infinity. Similarly, as long as the noise is uncorrelated to the channel coefficients, the $\frac{1}{M}\mathbf{G}^*(t)\mathbf{n}(t)$ in **Eq. (2.24)**, which can be viewed as correlation between the channel coefficients and the noise, approaches to zero with the increase of M. In [6], Marzetta points out that with the same number of users, more antennas at the base stations will always benefit the system to have a better SNR. When the number of antennas goes to infinity, the uncorrelated noise will be vanished.

The ZF algorithm, which was mentioned in previous section and is showed in **Eq. (2.25)**, further polishes the MRC algorithm. Instead of dividing the summation of rotated signals by the number of antennas M, ZF scales the signal by applying pseudo inverse of the channel coefficients matrix to the

signal.

$$\mathbf{D}(t) = \mathbf{G}^{\dagger}(t)\mathbf{y}(t),$$

$$\mathbf{D}(t) = \mathbf{G}^{\dagger}\sqrt{Pt}\mathbf{G}(t)\mathbf{x}(t) + \mathbf{G}^{\dagger}(t)\mathbf{n}(t), \tag{2.25}$$

where

$$\mathbf{G}^{\dagger}(t) = (\mathbf{G}^{*}(t)\mathbf{G}(t))^{-1}\mathbf{G}^{*}(t)$$

denotes the pseudo inverse of channel coefficients matrix $\mathbf{G}(t)$.

The condition number of the part $(\mathbf{G}^{*}(t)\mathbf{G}(t))$ will decrease inverse proportionally with the number of receiver antennas. For a base station using ZF recovery algorithm, the lower the channel matrix condition number is, the lower the power of the noise will be. When the condition number is as low as one, the noise part $\mathbf{G}^{\dagger}(t)\mathbf{n}(t)$, like MRC, can be viewed as correlation matrix of the channel coefficients and the noise. The noise part will approach zero with the increase of M as long as it is unrelated to channel coefficients. Note that the condition number in the matrix $\mathbf{G}(t)$ represents the channel diversity gain.

2.3.4 Inter-cell interference

Non-cooperative systems, which are considered in this thesis, work without communication with neighboring cells. It further implies that the pilot signals are assigned and will not change adaptively in order to avoid pilot contamination. Therefore, for systems that operate with frequency reuse factor

of one, every base station suffers from the interference from other cells during the training period. An inter cell interference (ICI) contaminated received signal can be expressed as,

$$\mathbf{y}_0(t) = \sqrt{P_0}\mathbf{G}_0(t)\mathbf{x}(t) + \sum_{l=1}^{L}\sqrt{P_l}\mathbf{G}_l(t)\mathbf{x}(t) + \mathbf{n}(t), \quad (2.26)$$

where $\mathbf{G}_0(t)$ is the channel coefficients matrix of the cell of interest and $\mathbf{G}_l(t),\ l = 1, 2, \ldots, L$ is the channel coefficients matrix from the interfering users in the l^{th} cell, $\mathbf{x}(t)$ is the pilot signal vector and $\mathbf{n}(t)$ is the system uncorrelated noise. P_0 and P_l are the transmission power of desired and interfering users, respectively. The channel coefficients matrix estimated from the pilot signal can be described by

$$\mathbf{G}_e(t) = \sqrt{P_0}\mathbf{G}_0(t) + \sum_{l=1}^{L}\sqrt{P_l}\mathbf{G}_l(t) + \mathbf{w}(t), \quad (2.27)$$

where $\mathbf{w}(t)$ is uncorrelated estimation noise matrix and $\sum_{l=1}^{L}\sqrt{P_l}\mathbf{G}_l(t)$ is the ICI channel estimation error matrix. Note that $\sum_{l=1}^{L}\sqrt{P_l}\mathbf{G}_l(t)$ is a Gaussian random matrix because $\sqrt{P_l}\mathbf{G}_l(t)$ are all independent Gaussian random matrices.

With inaccurate channel estimation, the received data signal after MRC algorithm will became,

$$\frac{1}{M}\mathbf{D}(t) = \frac{1}{M}(\sqrt{P_0}\mathbf{G}_0(t) + \sum_{l=1}^{L}\sqrt{P_l}\mathbf{G}_l(t))^*(\sqrt{P_0}\mathbf{G}(t)\mathbf{x}_0(t)$$

$$+ \sum_{l=1}^{L}\sqrt{P_l}\mathbf{G}_l(t)\mathbf{x}_l(t) + \frac{1}{M}\mathbf{G}^*(t)\mathbf{w}(t), \quad (2.28)$$

if the M is large enough,

$$\frac{1}{M}\mathbf{D}(t) \cong P_0\mathbf{x}_0(t) + \sum_{l=1}^{L} P_l\mathbf{G}_l(t)\,\mathbf{x}_l(t). \quad (2.29)$$

If we further assume the transmission power for all mobile users is same, **Eq. (2.29)** can be rewritten as

$$\frac{1}{M}\mathbf{D}(t) \cong x_0(t) + \sum_{l=1}^{L} \mathbf{G}_l(t)\,\mathbf{x}_l(t). \quad (2.30)$$

It is clear though with large number of receiver antennas, the error of the detected signal is mainly caused by the ICI. Note that if the data in $\mathbf{x}_l(t)$ is uniformly distributed, $\sum_{l=1}^{L} \mathbf{G}_l(t)\,\mathbf{x}_l(t)$ can also be viewed as a Gaussian noise.

2.4 Kalman Filters

2.4.1 Derivation of Kalman Filter

For any systems that can be formulated into the form,

$$\begin{cases} \mathbf{x}(t) = \mathbf{A}\,\mathbf{x}(t-1) + \mathbf{v}(t) \\ \mathbf{y}(t) = \mathbf{H}\,\mathbf{x}(t) + \mathbf{w}(t) \end{cases}, \quad (2.31)$$

where $\mathbf{x}(t)$ is the state, $\mathbf{y}(t)$ is the measurement, **A** and **H** are the state transition and measurement matrices, respectively; $\mathbf{v}(t)$ and $\mathbf{w}(t)$ are process noise and measurement noise, respectively. The process noise covariance and measurement noise covariance are given by

$$\mathbf{Q} = E[\mathbf{v}(t)\mathbf{v}(t)^T], \quad (2.32)$$

$$\mathbf{R} = \mathrm{E}[\mathbf{w}(\mathrm{t})\mathbf{w}(\mathrm{t})^{\mathrm{T}}], \tag{2.33}$$

respectively.

Define $\hat{\mathbf{x}}(\mathrm{t})$ as the estimate of $\mathbf{x}(\mathrm{t})$, therefore the estimate error can be written as,

$$\mathbf{e}(\mathrm{t}) = \mathbf{x}(\mathrm{t}) - \hat{\mathbf{x}}(\mathrm{t}). \tag{2.34}$$

Then, the error covariance matrix can be written as

$$\mathbf{P}(\mathrm{t}) = \mathrm{E}[\mathbf{e}(\mathrm{t})\mathbf{e}(\mathrm{t})^{\mathrm{T}}], \tag{2.35}$$

With a known process state transition matrix **A**, a prior estimate of $\mathbf{x}(\mathrm{t})$ can be generated by

$$\hat{\mathbf{x}}(\mathrm{t})^{-} = \mathbf{A}\,\hat{\mathbf{x}}(\mathrm{t}-1). \tag{2.36}$$

Then, a refined estimate with knowledge of measurement can be formulated as

$$\hat{\mathbf{x}}(\mathrm{t}) = \hat{\mathbf{x}}(\mathrm{t})^{-} + \mathbf{K}(\mathrm{t})(\mathbf{y}(\mathrm{t}) - \mathbf{H}\,\hat{\mathbf{x}}(\mathrm{t})^{-}). \tag{2.37}$$

Substituting **Eq. (2.30)** into **Eq. (2.37)**, yields

$$\hat{\mathbf{x}}(\mathrm{t}) = \hat{\mathbf{x}}(\mathrm{t})^{-} + \mathbf{K}(\mathrm{t})(\mathbf{H}\,\mathbf{x}(\mathrm{t}) + \mathbf{w}(\mathrm{t}) - \mathbf{H}\,\hat{\mathbf{x}}(\mathrm{t})^{-}), \tag{2.38}$$

where $\mathbf{K}(\mathrm{t})$ is the Kalman gain at time t. Then the error becomes

$$\mathbf{e}(\mathrm{t}) = \hat{\mathbf{x}}(\mathrm{t}) - \mathbf{x}(\mathrm{t}) = (\mathbf{I} - \mathbf{K}(\mathrm{t})\mathbf{H})\hat{\mathbf{x}}(\mathrm{t})^{-} + (\mathbf{K}(\mathrm{t})\mathbf{H} - \mathbf{I})\,\mathbf{x}(\mathrm{t}) + \mathbf{K}(\mathrm{t})\mathbf{w}(\mathrm{t}). \tag{2.39}$$

Substituting the error vector into the error covariance matrix $\mathbf{P}(t)$, we get

$$\mathbf{P}(t) = (\mathbf{I} - \mathbf{K}(t)\mathbf{H})\mathbf{E}\left[\left(\hat{\mathbf{x}}(t)^{-} - \mathbf{x}(t)\right)\left(\hat{\mathbf{x}}(t)^{-} - \mathbf{x}(t)\right)^{T}\right](\mathbf{I} - \mathbf{K}(t)\mathbf{H})^{T}$$

$$+\mathbf{K}(t)\mathrm{E}[\mathbf{w}(t)\mathbf{w}(t)^{T}]\mathbf{K}(t)^{T}, \quad (2.40)$$

Let

$$\mathbf{P}(t)^{-} = \mathrm{E}\left[\left(\hat{\mathbf{x}}(t)^{-} - \mathbf{x}(t)\right)\left(\hat{\mathbf{x}}(t)^{-} - \mathbf{x}(t)\right)^{T}\right], \quad (2.41)$$

denote the prior error covariance matrix. Substituting **Eq. (2.31)** into **Eq. (2.38)**, yields

$$\mathbf{P}(t) = (\mathbf{I} - \mathbf{K}(t)\mathbf{H})\mathbf{P}(t)^{-}(\mathbf{I} - \mathbf{K}(t)\mathbf{H})^{T} + \mathbf{K}(t)\,\mathbf{R}\,\mathbf{K}(t)^{T}, \quad (2.42)$$

$$\mathbf{P}(t) = \mathbf{P}(t)^{-} - \mathbf{K}(t)\mathbf{H}\mathbf{P}(t)^{-} - (\mathbf{K}(t)\mathbf{H}\mathbf{P}(t)^{-})^{T}$$

$$+\mathbf{K}(t)\,(\mathbf{R} + \mathbf{H}\mathbf{P}(t)^{-}\mathbf{H}^{T})\,\mathbf{K}(t)^{T}. \quad (2.43)$$

Note that each element in the trace of $\mathbf{P}(t)$ is the mean square error (MSE) of each element in the state estimate $\hat{\mathbf{x}}(t)$. Taking the derivative of trace of $\mathbf{P}(t)$ in order to minimize the MSE of the estimated state

$$\frac{\mathrm{d}Tr(\mathbf{P}(t))}{\mathrm{d}\mathbf{K}(t)} = -2\mathbf{H}\mathbf{P}(t)^{-} + 2\mathbf{K}(t)\,(\mathbf{R} + \mathbf{H}\mathbf{P}(t)^{-}\mathbf{H}^{T}), \quad (2.44)$$

and setting it to zero,

$$-2\mathbf{H}\mathbf{P}(t)^{-} + 2\mathbf{K}(t)\,(\mathbf{R} + \mathbf{H}\mathrm{P}(t)^{-}\mathbf{H}^{T}) = 0, \quad (2.45)$$

yields the Kalman gain

$$\mathbf{K}(\mathrm{t}) = \mathbf{H}\mathbf{P}(\mathrm{t})^{-}(\mathbf{R} + \mathbf{H}\mathbf{P}(\mathrm{t})^{-}\mathbf{H}^{\mathrm{T}})^{-1}. \tag{2.46}$$

Substituting **Eq. (2.46)** into **Eq. (2.43)** gives the error covariance matrix

$$\mathbf{P}(\mathrm{t}) = (\mathbf{I} - \mathbf{K}(\mathrm{t})\mathbf{H})\mathbf{P}(\mathrm{t})^{-}, \tag{2.47}$$

and the prior error covariance matrix updates from previous time slot as

$$\mathbf{P}(\mathrm{t}+1)^{-} = \mathrm{E}[\left(\mathbf{A}\hat{\mathbf{x}}(\mathrm{t}) - \mathbf{x}(\mathrm{t}+1)\right)\left(\mathbf{A}\hat{\mathbf{x}}(\mathrm{t}) - \mathbf{x}(\mathrm{t}+1)\right)^{\mathrm{T}}]$$

$$\mathbf{P}(\mathrm{t}+1)^{-} = \mathrm{E}[(\mathbf{A}\hat{\mathbf{x}}(\mathrm{t}) - \mathbf{A}\mathbf{x}(\mathrm{t}) - \mathbf{v}(\mathrm{t}))(\mathbf{A}\hat{\mathbf{x}}(\mathrm{t}) - \mathbf{A}\mathbf{x}(\mathrm{t}) - \mathbf{v}(\mathrm{t}))^{\mathrm{T}}]$$

$$\mathbf{P}(\mathrm{t}+1)^{-} = \mathbf{A}\,\mathrm{E}[\left(\hat{\mathbf{x}}(\mathrm{t}) - \mathbf{x}(\mathrm{t})\right)\left(\hat{\mathbf{x}}(\mathrm{t}) - \mathbf{x}(\mathrm{t})\right)^{\mathrm{T}}]\mathbf{A}^{\mathrm{T}} + \mathrm{E}[\mathbf{v}(\mathrm{t})\mathbf{v}(\mathrm{t})^{\mathrm{T}}]$$

$$\mathbf{P}(\mathrm{t}+1)^{-} = \mathbf{A}\,\mathbf{P}(\mathrm{t})\mathbf{A}^{\mathrm{T}} + \mathbf{Q}. \tag{2.48}$$

The recursive Kalman filter algorithm can be summarized [15]

1) Time Update:

$$\hat{\mathbf{x}}(\mathrm{t})^{-} = \mathbf{A}\,\hat{\mathbf{x}}(\mathrm{t}-1) \tag{2.49}$$

$$\mathbf{P}(\mathrm{t})^{-} = \mathbf{A}\,\mathbf{P}(\mathrm{t}-1)\mathbf{A}^{\mathrm{T}} + \mathbf{Q} \tag{2.50}$$

2) Measurement Update

$$\mathbf{K}(\mathrm{t}) = \mathbf{H}\mathbf{P}(\mathrm{t})^{-}(\mathbf{R} + \mathbf{H}\mathbf{P}(\mathrm{t})^{-}\mathbf{H}^{\mathrm{T}})^{-1} \tag{2.51}$$

$$\hat{\mathbf{x}}(t) = \hat{\mathbf{x}}(t)^{-} + \mathbf{K}(t)(\mathbf{y}(t) - \mathbf{H}\,\hat{\mathbf{x}}(t)^{-}) \quad (2.52)$$

$$\mathbf{P}(t) = (\mathbf{I} - \mathbf{K}(t)\mathbf{H})\mathbf{P}(t)^{-} \quad (2.53)$$

2.4.2 Advantages and Limitations of Kalman Filter

The derivation in the previous section shows that the discrete-time Kalman filter is a recursive state MSE minimizer for linear systems. Given the fact that a summation of two independent Gaussian random variables is also a Gaussian random variable, if a linear system contains only independent Gaussian process noise and measurement noise, and the state is a scalar, the state estimate $\hat{x}(t)$ of KF will be the maximum likelihood estimate. The KF therefore is considered as an optimal filter for linear systems with independent Gaussian noise. Additionally, the KF does not require invertible measurement matrix H, which is very convenient for a recursive state estimator. This property allows the measurement vector to be smaller than the state vector. However, the KF requires exact linear transition function and known covariance matrix for both process noise and measurement noise. Therefore, KF has to be modified before to perform the estimation of the state of non-linear systems or systems with dynamic transition matrix.

3 System Modeling

3.1 Measurement Model

We consider the uplink of a Massive MIMO system, which has M base station antennas and K single antenna mobile users. We also assume a time varying and frequency nonselective channel and a narrow band information signal so that we can represent the system model as a single tap at each instant of time. In the worst case scenario, all users communicate with the base station simultaneously. Under these assumptions, the received signal at the base station of the cell of interest (Cell 0) can be described by

$$\mathbf{y}_0(t) = \sqrt{Pt}\mathbf{G_0}(t)\mathbf{x}_0(t) + \mathbf{n}(t) + \mathbf{I}(t), \tag{3.1}$$

where P_t is the transmitted power, $\mathbf{y}_0(t)$ is a $M \times 1$ vector of the received signals at base station, $\mathbf{x}_0(t)$ is a $K \times 1$ vector of simultaneously transmitted signals by K independent mobile users from the cell of interest, $\mathbf{n}(t)$ is a $M \times 1$ vector representing the i.i.d. additive zero-mean white Gaussian noise with variance σ_n^2 and $\mathbf{G_0}(t)$ is the $M \times K$ channel coefficients matrix. An element lies on i-th row and j-th column of $\mathbf{G_0}(t)$ is denoted by $g_{i,j}(t)$, corresponding to channel coefficient between i-th receiving antenna and j-th transmitting antenna at time t. $\mathbf{I}(t)$, which is introduced in **Eq. (2.24)** $\sum_{l=1}^{L} \sqrt{P_l}\mathbf{G}_l(t)\mathbf{x}_l(t)$, is referred to as the ICI which is caused by other users transmitting from neighboring cells. The ICI can be viewed as an uncorrelated noise at receiver during the data transmission process. However, it becomes

correlated noise during training process.

The propagation coefficient $g_{i,j}(t)$ is usually modeled as a product of a small scale and a large scale fading coefficients, i.e.

$$g_{i,j}(t) = h_{i,j}(t) \cdot \beta_{jl}^{1/2}, \tag{3.2}$$

where $h_{i,j}(t)$ is the small scale fading coefficient and is assumed to be zero-mean complex Gaussian with each component having unit variance. Under the Rayleigh fading channel assumption, the envelop of a small scale fading coefficient is a Rayleigh distributed random variable. The second factor $\beta_{jl}^{1/2}$ is the large scale fading coefficient between j^{th} user and l^{th} base station and this coefficient is assumed to be identical between all the base station antennas to one mobile device. Generally it can be expressed as

$$\beta_{jl}^{1/2} = \frac{z_{jl}}{r_{jl}^{\gamma}}, \tag{3.3}$$

where r_j is the distance between the j-th user and the l^{th} base station, γ is the decay exponent of the cell of interest. The numerator z_{jl} is the shadowing factor and it is a log-normal random variable which only depends on the location of the j-th user [6]. After conversion to decibel, $10\log_{10} Z_{jl}$ is a zero-mean Gaussian random variable with standard deviation of σ_{shad}. Because the shadowing factor z and distance r change slowly over time, the large scale fading factor is therefore modeled as a constant. Hence, for each communication period, the large scale fading coefficient is usually assumed to

be constant. Given the fact that large scale fading factors are amplitude scaling factors, it could be estimated using the amplitude attenuation of the pilot signal. Thus, we consider the large scale fading matrix between the base station and the users in the cell of interest as a known constant diagonal matrix, namely,

$$\beta_{ll}^{1/2} = \begin{bmatrix} \beta_{1l}^{1/2} & 0 & \cdots & \cdots & 0 \\ 0 & \beta_{2l}^{1/2} & 0 & \cdots & 0 \\ 0 & 0 & \ddots & & \vdots \\ \vdots & \vdots & & \ddots & 0 \\ 0 & 0 & \cdots & 0 & \beta_{Kl}^{1/2} \end{bmatrix}. \tag{3.4}$$

Hence, we can compensate for the large scale fading factor and rewrite the received signal as

$$\mathbf{y}(t) = \mathbf{H}(t)\mathbf{x}(t) + \mathbf{w}(t) + \mathbf{I}(t), \tag{3.5}$$

where $\mathbf{H}(t)$ is a $M \times K$ matrix where the element which lies on i-th row and j-th column is denoted by $h_{i,j}(t)$, corresponding to the channel small scale fading coefficient between i-th receiving antenna and j-th transmitting antenna at time t. $I(t)$ represents the baseband ICI, which at the same time is scaled by the large scale fading coefficients that decay with the separation distance between transmitter and receiver, i.e.

$$\mathbf{I}(t) = \sum_{l=1}^{L} \sqrt{P_l} \frac{\beta_l}{\beta_0} \mathbf{H}_l(t)\mathbf{x}(t), \tag{3.6}$$

where $\frac{\beta_l(t)}{\beta_0(t)}$ is the average large scale fading factor ratio of the neighboring cells' users to the users in the cell of interest, which directly influences the power of ICI. If the transmission power is normalized to 1, the variance of each

ICI component is $\frac{\beta_l(t)}{\beta_0(t)}$. If we assume the number of neighboring cells is 6 and the average distance of an interfering user from each neighboring cell is same, then, the ICI is a complex Gaussian random matrix with zero mean and variance of $\frac{6\beta_l(t)}{\beta_0(t)}$. A very common model for large scale fading coefficients is called slope intercept model [25]

$$\text{Path Loss (dB)} = 10\log_{10}(\beta) = -\alpha - b \cdot \log_{10}(r), \quad (3.7)$$

where r is the distance between the transmitter and receiver, α and b are the parameters determined by the model [25]. In an urban microcell non-LOS area, path loss can be described as [30]

$$\text{Path Loss (dB)} = -55.9 + \left(24.5 + \frac{f_c}{616.67}\right)\log_{10}(f_c) + 38\log_{10}(r), \quad (3.8)$$

where f_c is the carrier frequency. Thus, the variance of each ICI component can be expressed as

$$10\log_{10}\left(\frac{\beta_l(t)}{\beta_0(t)}\right) = 38\log(r_l) - 38\log(r_0), \quad (3.9)$$

where r_0 is the distance between the user in the cell of interest and the base station in the cell of interest and r_l is the distance between the user in the neighboring cell and the base station in the cell of interest.

The relationship between received, transmitted signal and fast fading channel coefficients matrix is well expressed in **Eq. (3.5)**. Therefore, **Eq. (3.5)** can be viewed as a linear measurement equation of the system.

3.2 Channel Dynamic Model

Due to the motion between the mobile transmitter and the base station receiver antennas, the channel fast fading coefficients are changing rapidly with time. The theoretical derivation of the channel autocorrelation factor was presented in the previous chapter. In order to maintain simplicity, we further approximate **Eq. (2.20)** as

$$E[h_{i,j}(t) * h_{i,j}^{*}(t+\tau)] \approx J_0(2\pi f_D \tau), \tag{3.10}$$

Given that the channel coefficients are not constant, we need to track the channel in real-time in order to improve data detection. In this work, we adopt the widely used first order stationary Gauss-Markov process [31][32][33] to represent the channel dynamics, namely,

$$\mathbf{H}(t+1) = a(t+1) * \mathbf{H}(t) + \sqrt{1 - a^2(t)}\,\mathbf{B}(t+1). \tag{3.11}$$

where $a(t)$ is the channel autocorrelation factor vector at time t and the matrix $\mathbf{B}(t+1)$ has unit variance zero-mean complex Gaussian random entries. Therefore, **Eq. (3.11)** can be viewed as the state transition equation of the system. When $a(t)$ is constant, the system is linear system. Otherwise, the system will be no longer linear if $a(t)$ is time varying.

4 Problem and Proposed Solution

4.1 Channel Estimation Based on Kalman Filter

Given that we have assumed the channel is changing rapidly during one frame, we cannot recover our transmitted data accurately based on the constant channel coefficient matrices, which are obtained from the reference pilot signal at the beginning of each frame. Thus, a real-time channel coefficients tracker which keeps the estimated channel coefficients updated during each frame is important. The KF is an excellent candidate to track channel fast fading coefficients [16]. As described in **Chapter 2**, the KF is a linear filter which can reduce the effects of the random system process noise and the measurement noise, recursively. Here, we will build a real-time channel fast fading coefficient estimator based on KF. To do this, we shall use **Eqs. (3.5)** and **(3.11)** to construct a state model of the massive MIMO uplink communication system in the form of a state transition equation and a measurement equation that matches the Kalman filter form

$$\begin{cases} \mathbf{H}(\mathrm{t}+1) = \mathbf{A} * \mathbf{H}(\mathrm{t}) + (\mathbf{I} - \mathbf{A}\mathbf{A}^{\mathrm{T}})^{\frac{1}{2}}\mathbf{B}(\mathrm{t}+1) \\ \mathbf{y}(\mathrm{t}+1) = \mathbf{H}(\mathrm{t}+1)\mathbf{x}(\mathrm{t}+1) + \mathbf{n}(\mathrm{t}+1) + \mathbf{I}(\mathrm{t}+1) \end{cases}, \tag{4.1}$$

where $\mathbf{A}$ is a diagonal matrix whose each diagonal element is the channel autocorrelation associated with each mobile user, $(\mathbf{I} - \mathbf{A}\mathbf{A}^{\mathrm{T}})\mathbf{B}(\mathrm{t}+1)$ is the system process noise matrix, $\mathbf{B}(\mathrm{t}+1)$ is a complex Gaussian random matrix with zero-mean and unit variance entries, $\mathbf{n}(\mathrm{t}+1) + \mathbf{I}(\mathrm{t}+1)$ is the measurement noise that contains measurement noise $\mathbf{n}(\mathrm{t}+1)$ and the ICI

$\mathbf{I}(t+1)$. Note that both $\mathbf{X}(t)$ and $\mathbf{H}(t)$ are unknown in this system representation. In order to run the Kalman filter successfully, the previous channel coefficient $\mathbf{H}(t-1)$ is used to recover the data $\mathbf{x}(t)$ and then substitute $\mathbf{x}(t)$ into measurement equation to recover the channel coefficients matrix as a measurement matrix. The ZF algorithm is chosen to be the receiver algorithm due to its low computational complexity.

$$\mathbf{x}(t) = \mathbf{H}_e^{-\dagger}(t)\mathbf{y}(t). \tag{4.2}$$

where $\mathbf{H}_e^{-\dagger}$ denotes the pseudo inverse of the estimated channel coefficients matrix after Kalman filter time update step. Any nonlinear receiver algorithm such as maximum likelihood (ML) is too computationally complex for a real time recursive algorithm, even though it generally has better performance. Besides, massive MIMO systems provide very high channel diversity that grows proportional the number of receiver antennas that makes the ZF become comparable to nonlinear receiver algorithms in performance.

After $\mathbf{x}(t)$ has been estimated, we can treat it as a measurement matrix that measuring channel coefficients matrix $\mathbf{H}(t)$. Therefore, we can rewrite **Eq. (4.1)** as

$$\begin{cases} \mathbf{h}(t+1) = \mathbf{A} * \mathbf{h}(t) + (\mathbf{I} - \mathbf{A}\mathbf{A}^{T})^{\frac{1}{2}}\mathbf{B}(t+1) \\ \mathbf{y}(t+1) = \overline{\mathbf{X}}(t)\mathbf{h}(t) + \mathbf{n}(t+1) + \mathbf{I}(t+1) \end{cases}, \tag{4.3}$$

where

$$\mathbf{h}(t) = \mathrm{Vec}(\mathbf{H}(t)), \tag{4.4}$$

$$\overline{\mathbf{X}}(\mathrm{t}) = \mathbf{x}^{\mathrm{T}}(\mathrm{t}) \otimes \mathbf{I}_{\mathrm{M}}. \tag{4.5}$$

$\mathrm{Vec}(\cdot)$ denotes the vectorization transformation and $\otimes$ denotes the Kronecker product. The vector $\mathbf{h}(\mathrm{t})$ is therefore the vectorized channel coefficient matrix, which is the system state vector to be estimated.

Now, **Eq. (4.5)** matches the standard Kalman filter form and we can use the Kalman filter to track the channel fast fading coefficients matrix recursively. The channel coefficients estimator based on Kalman filter can be summarized as follows:

3) Time Update:

$$\hat{\mathbf{h}}(\mathrm{t})^{-} = \mathbf{A}\,\hat{\mathbf{h}}(\mathrm{t}-1), \tag{4.6}$$

$$\mathbf{P}(\mathrm{t})^{-} = \mathbf{A}\,\mathbf{P}(\mathrm{t}-1)\,\mathbf{A}^{\mathrm{T}} + \mathbf{Q}, \tag{4.7}$$

4) Data Detection:

$$\mathbf{x}(\mathrm{t}) = \mathbf{H}_{\mathrm{e}}^{-\dagger}(\mathrm{t})\mathbf{y}(\mathrm{t}), \tag{4.8}$$

$$\overline{\mathbf{X}}(\mathrm{t}) = \mathbf{x}^{\mathrm{T}}(\mathrm{t}) \otimes \mathbf{I}_{\mathrm{M}}, \tag{4.9}$$

5) Measurement Update

$$\mathbf{K}(\mathrm{t}) = \overline{\mathbf{X}}(\mathrm{t})\mathbf{P}(\mathrm{t})^{-}\left(\mathbf{R} + \overline{\mathbf{X}}(\mathrm{t})\mathbf{P}(\mathrm{t})^{-}\overline{\mathbf{X}}(\mathrm{t})^{\mathrm{T}}\right)^{-1} \tag{4.10}$$

$$\hat{\mathbf{h}}(\mathrm{t}) = \hat{\mathbf{h}}(\mathrm{t})^{-} + \mathbf{K}(\mathrm{t})(\mathbf{y}(\mathrm{t}) - \overline{\mathbf{X}}(\mathrm{t})\,\hat{\mathbf{h}}(\mathrm{t})^{-}) \tag{4.11}$$

$$\mathbf{P}(t) = \left(\mathbf{I} - \mathbf{K}(t)\overline{\mathbf{X}}(t)\right)\mathbf{P}(t)^{-} \tag{4.12}$$

Note that, because this is a real time filter, any error in one step will possibly lead to a series of errors in the following steps with high probability.

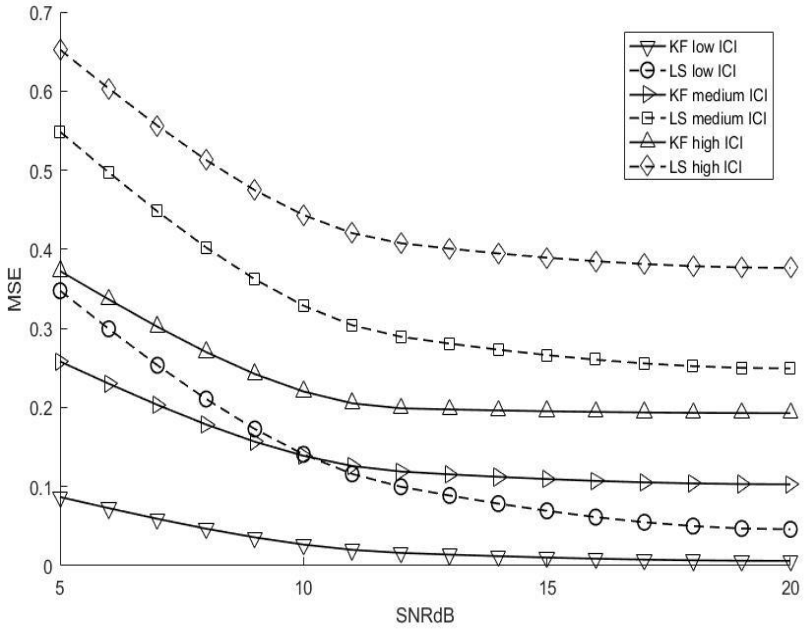

Figure 4.1 Performance comparison between Kalman filter and LS method.

Fig. 4.1 shows the channel estimation MSE produced by the Kalman filter channel estimator and the LS method under different levels of inter-cell interference power. From the figure we can observe that Kalman filter can better deal with the influence of ICI.

4.2 Problem of Traditional Method

The traditional channel estimation method based on Kalman filter assumes that the channel fast fading coefficients vary linearly. A linearly changing channel

environment is considered based on the assumptions that motion between the transmitting antennas and the receiving antennas are constant. However, in practice, vehicles are not moving at constant speed, especially in the urban areas. During the vehicles' acceleration or deceleration, the channel fast fading coefficients do not change linearly. Namely, the channel autocorrelation factor $a(t)$ is not a constant.

The KF tracking scheme presented in the previous section is based on the linear dynamic channel assumption. In a nonlinear environment, traditional KF method may not perform well. Therefore, we modify the KF using a time varying $a(t)$. The performance curves are shown in **Fig. 4.2**.

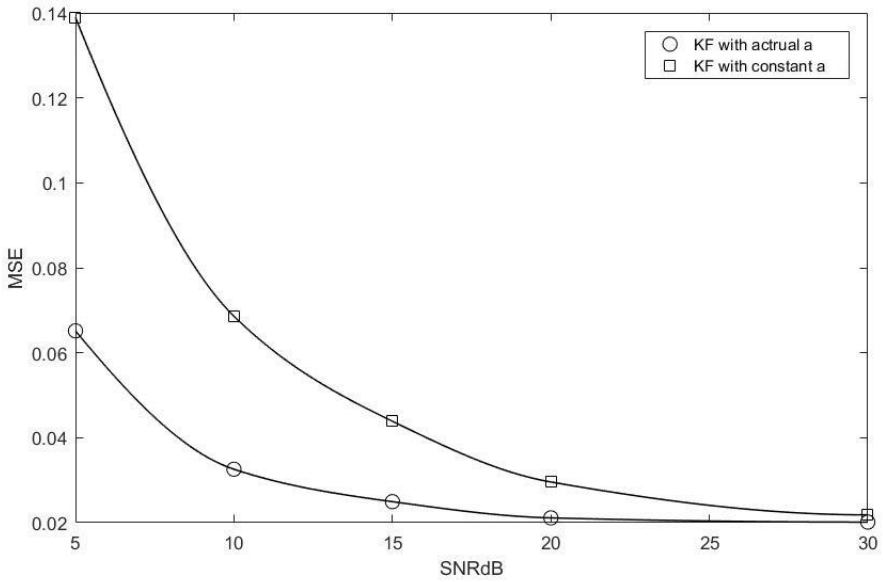

Figure 4.2 Comparison of KF with constant and actual a.

The gap between the performance of Kalman filter with actual channel autocorrelation and with constant autocorrelation can be easily observed in **Fig. 4.2**. It reveals the importance of accurate channel autocorrelation factor in

Kalman filter channel estimation. For the purpose of enhancing the robustness of channel coefficients estimator, the channel autocorrelation need to be accurately estimated. We design two combined channel coefficients and channel autocorrelation estimator based on Kalman filter and LS in ensuing section.

4.3 Suggested Solution and Simulation

The performance gap shown in **Fig. 4.2** is due to the fact that channel autocorrelation factor $a(t)$ is not constant between pilot signals. In order to improve the accuracy of channel coefficients estimation, we designed two estimators that track both channel autocorrelation and channel coefficients between reference signals simultaneously. First, we modified the traditional Kalman filter with autocorrelation estimator based on LS. Then, we design an augmented Kalman filter channel estimator, which contains a channel coefficients matrix estimator and an autocorrelation factor estimator.

4.3.1 Combined Autocorrelation and Channel Estimator based on Kalman Filter and LS Method

Assuming $a(t)$ is not a constant between two reference pilot signals, we adopt the widely used random walk model for $a(t)$ to formulate the algorithm [19].

$$a(t+1) = a(t) + \varepsilon_a \tag{4.13}$$

where ε_a is a zero mean Gaussian random noise, which denotes the process noise of $a(t)$. We also adopt a first order auto regressive model to represent the

channel fast fading coefficient dynamics.

$$\mathbf{H}(\mathrm{t}+1) = \mathbf{A}(\mathrm{t}+1) \cdot \mathbf{H}(\mathrm{t}) + (\mathbf{I} - \mathbf{A}(\mathrm{t})\mathbf{A}(\mathrm{t})^{\mathrm{T}})^{\frac{1}{2}} \mathbf{B}(\mathrm{t}+1). \qquad (4.14)$$

Post multiplying by $\mathbf{H}(\mathrm{t})^{\dagger}$ to both sides of **Eq. (4.7)**, yields

$$\mathbf{H}(\mathrm{t}+1)\mathbf{H}(\mathrm{t})^{\dagger} = \mathbf{A}(\mathrm{t}+1) + (\mathbf{I} - \mathbf{A}(\mathrm{t})\mathbf{A}(\mathrm{t})^{\mathrm{T}})^{\frac{1}{2}} \mathbf{B}(\mathrm{t}+1)\mathbf{H}(\mathrm{t})^{\dagger}. \quad (4.15)$$

Due to the fact that $\mathbf{B}(\mathrm{t}+1)$ and $\mathbf{H}(\mathrm{t})$ are uncorrelated Gaussian random matrices, the noise term $\mathbf{B}(\mathrm{t}+1)\mathbf{H}(\mathrm{t})^{\dagger}$ decreases with the increase of the number of antennas at the receiver side. Let us first test this LS autocorrelation estimator using true channel coefficients to evaluate the feasibility of this method.

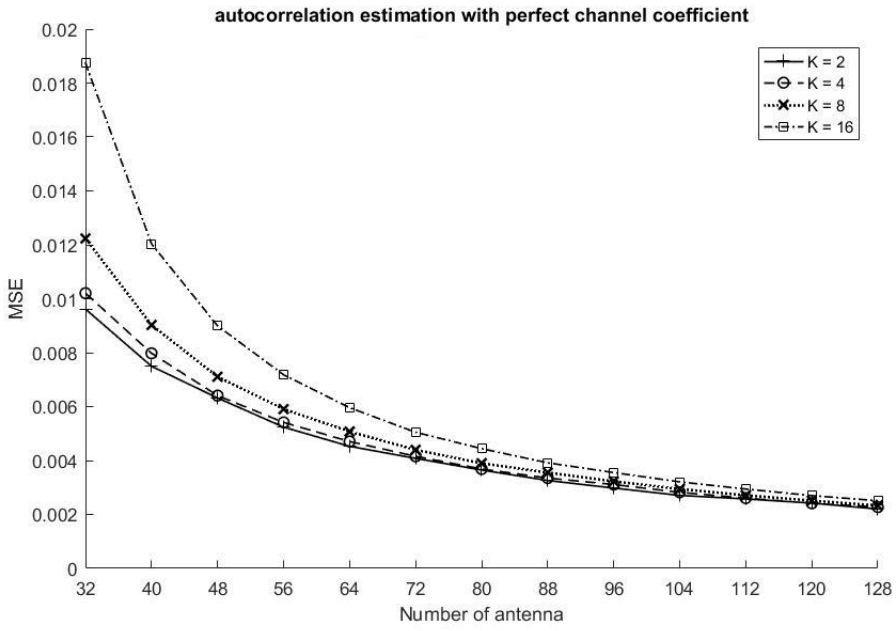

Figure 4.3 Channel autocorrelation estimation with actual channel coefficients.

Fig. 4.3 shows the performance of autocorrelation estimator versus the number

of antennas at the receiver side. Curves with different line types represent the different number of antennas at transmitter. The performance of the estimator improves with the increase of the number of antennas. However, the decreasing rate of the estimator's MSE gets slower with the increase of the receiver antennas. Therefore, continuing increase of the receiver antennas will not give desirable performance gain.

In practice, accurate channel coefficients are not available, because the estimate error can never be totally eliminated. Let us fix the K to 4 and test the LS method with estimated channel coefficients that contain noise of different levels. The results are shown in **Fig. 4.4**.

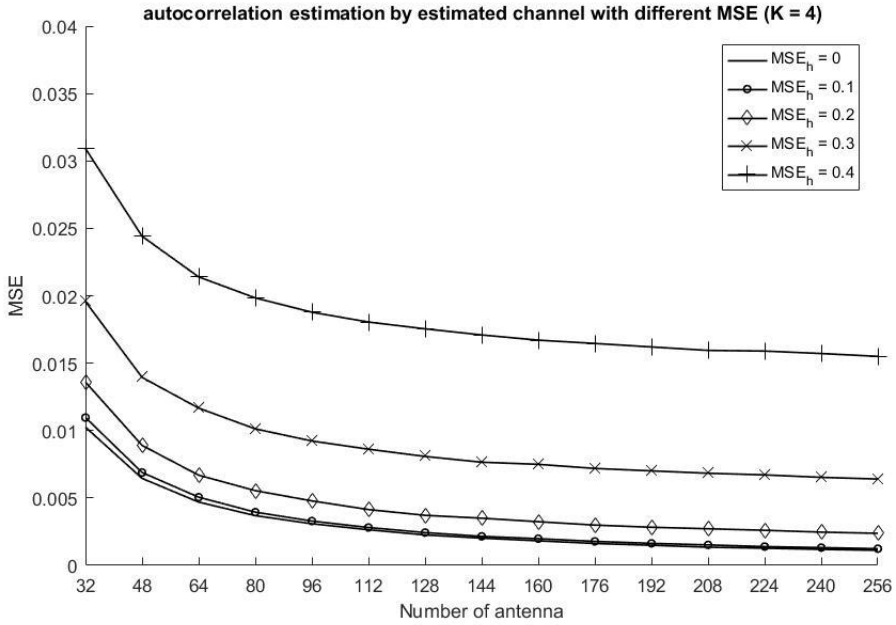

Figure 4.4 Channel autocorrelation estimation with estimated channel coefficients.

Fig. 4.4 clearly shows how the error of estimated channel coefficient influences

performance of the autocorrelation estimation. It shows that the LS estimator will get worse quickly when the MSE of the channel coefficient estimation is greater than 0.2. It implies that the combined Kalman and LS channel coefficient estimator is sensitive to the SNR.

The combined estimator is now summarized

1) Time Update:

$$\hat{\mathbf{h}}(\mathrm{t})^{-} = \mathbf{A}_{\mathrm{e}}(\mathrm{t}-1)\,\hat{\mathbf{h}}(\mathrm{t}-1) \tag{4.16}$$

$$\mathbf{P}(\mathrm{t})^{-} = \mathbf{A}_{\mathrm{e}}(\mathrm{t})\,\mathbf{P}(\mathrm{t}-1)\,\mathbf{A}_{\mathrm{e}}(\mathrm{t})^{\mathrm{T}} + \mathbf{Q} \tag{4.17}$$

2) Data Detection:

$$\mathbf{x}(\mathrm{t}) = \mathbf{H}_{\mathrm{e}}^{-\dagger}(\mathrm{t})\mathbf{y}(\mathrm{t}) \tag{4.18}$$

$$\overline{\mathbf{X}}(\mathrm{t}) = \mathbf{x}^{\mathrm{T}}(\mathrm{t}) \otimes \mathbf{I}_{\mathrm{M}} \tag{4.19}$$

3) Measurement Update

$$\mathbf{K}(\mathrm{t}) = \overline{\mathbf{X}}(\mathrm{t})\mathbf{P}(\mathrm{t})^{-}\left(\mathbf{R} + \overline{\mathbf{X}}(\mathrm{t})\mathbf{P}(\mathrm{t})^{-}\overline{\mathbf{X}}(\mathrm{t})^{\mathrm{T}}\right)^{-1} \tag{4.20}$$

$$\hat{\mathbf{h}}(\mathrm{t}) = \hat{\mathbf{h}}(\mathrm{t})^{-} + \mathbf{K}(\mathrm{t})(\mathbf{y}(\mathrm{t}) - \overline{\mathbf{X}}(\mathrm{t})\,\hat{\mathbf{h}}(\mathrm{t})^{-}) \tag{4.21}$$

$$\mathbf{P}(\mathrm{t}) = \left(\mathbf{I} - \mathbf{K}(\mathrm{t})\overline{\mathbf{X}}(\mathrm{t})\right)\mathbf{P}(\mathrm{t})^{-} \tag{4.22}$$

$$\mathbf{A}_{\mathrm{e}}(\mathrm{t}) = \mathbf{H}_{\mathrm{e}}(\mathrm{t})\mathbf{H}_{\mathrm{e}}(\mathrm{t}-1)^{\dagger} \tag{4.23}$$

Note that the channel autocorrelation estimator and channel coefficients estimator is influenced by each other. Therefore, the accuracy of the channel autocorrelation estimation is very important. An error that is too large will cause the channel coefficients estimator perform worse and possibly result in a divergent of the autocorrelation estimator.

4.3.2 Combined Kalman Filters for Channel Autocorrelation and Channel Coefficients Estimation

In order to enhance the robustness of the autocorrelation estimator, the divergence of the autocorrelation estimation due to the channel coefficients estimation error need to be constrained. **Eqs. (4.13)** and **(4.14)** can be used as state transition and measurement equations, respectively, to perform Kalman filter estimation. The autocorrelation random walk system can be expressed as

$$\begin{cases} \mathbf{A}(t+1) = \mathbf{A}(t) + \boldsymbol{\varepsilon}_a \\ \mathbf{H}_e(t+1) = \mathbf{A}(t+1) * \mathbf{H}_e(t) + \mathbf{V}_a\, \mathbf{B}(t+1)' \end{cases} \tag{4.24}$$

where $\mathbf{V}_a$ is a $K \times K$ diagonal matrix, which each diagonal element is $\sqrt{1 - a_k{}^2(t)}$. a_k corresponds to the channel autocorrelation of the k^{th} mobile user. $\mathbf{H}_e(t)$ is the estimated channel coefficients matrix. And the combined channel correlation and channel coefficient estimator is now summarized

1) Time Update:

$$\hat{\mathbf{h}}(t)^- = \mathbf{A}_e(t)\, \hat{\mathbf{h}}(t-1) \tag{4.25}$$

$$\mathbf{P}(t)^- = \mathbf{A}_e(t)\, \mathbf{P}(t-1)\, \mathbf{A}_e(t)^T + \mathbf{Q} \tag{4.26}$$

2) Data Detection:

$$\mathbf{x}(\mathrm{t}) = \mathbf{H}_{\mathrm{e}}^{-\dagger}(\mathrm{t})\mathbf{y}(\mathrm{t}) \tag{4.27}$$

$$\overline{\mathbf{X}}(\mathrm{t}) = \mathbf{x}^{\mathrm{T}}(\mathrm{t}) \otimes \mathbf{I}_{\mathrm{M}} \tag{4.28}$$

3) Measurement Update

$$\mathbf{K}(\mathrm{t}) = \overline{\mathbf{X}}(\mathrm{t})\mathbf{P}(\mathrm{t})^{-}\left(\mathbf{R} + \overline{\mathbf{X}}(\mathrm{t})\mathbf{P}(\mathrm{t})^{-}\overline{\mathbf{X}}(\mathrm{t})^{\mathrm{T}}\right)^{-1} \tag{4.29}$$

$$\hat{\mathbf{h}}(\mathrm{t}) = \hat{\mathbf{h}}(\mathrm{t})^{-} + \mathbf{K}(\mathrm{t})(\mathbf{y}(\mathrm{t}) - \overline{\mathbf{X}}(\mathrm{t})\,\hat{\mathbf{h}}(\mathrm{t})^{-}) \tag{4.30}$$

$$\mathbf{P}(\mathrm{t}) = \left(\mathbf{I} - \mathbf{K}(\mathrm{t})\overline{\mathbf{X}}(\mathrm{t})\right)\mathbf{P}(\mathrm{t})^{-} \tag{4.31}$$

4) Autocorrelation Estimator

$$\mathbf{a}_e(\mathrm{t})^{-} = \mathbf{a}_e(\mathrm{t}-1) \tag{4.32}$$

$$\mathbf{P}_{\mathrm{a}}(\mathrm{t})^{-} = \mathbf{P}_{\mathrm{a}}(\mathrm{t}-1) + \mathbf{Q}_{\mathrm{a}} \tag{4.33}$$

$$\mathbf{K}_{\mathrm{a}}(\mathrm{t}) = \mathbf{H}_{\mathrm{e}}(\mathrm{t}-1)\mathbf{P}_{\mathrm{a}}(\mathrm{t})^{-}(\mathbf{R}_{\mathrm{a}} + \mathbf{H}_{\mathrm{e}}(\mathrm{t}-1)\mathbf{P}_{\mathrm{a}}(\mathrm{t})^{-}\mathbf{H}_{\mathrm{e}}(\mathrm{t}-1)^{\mathrm{T}})^{-1} \tag{4.34}$$

$$\mathbf{a}_e(\mathrm{t}) = \mathbf{a}_e(\mathrm{t})^{-} + \mathbf{K}_{\mathrm{a}}(\mathrm{t})(\mathbf{H}_{\mathrm{e}}(\mathrm{t}) - \mathbf{H}_{\mathrm{e}}(\mathrm{t}-1)\mathbf{a}_e(\mathrm{t})^{-}) \tag{4.35}$$

$$\mathbf{P}_{\mathrm{a}}(\mathrm{t}) = \left(\mathbf{I} - \mathbf{K}_{\mathrm{a}}(\mathrm{t})\mathbf{H}_{\mathrm{e}}(\mathrm{t}-1)\right)\mathbf{P}_{\mathrm{a}}(\mathrm{t})^{-} \tag{4.36}$$

where $\mathbf{a}_e$ is the channel autocorrelation vector which contains autocorrelation for all mobile users. The computational complexity of the proposed method is similar to traditional Kalman filter.

4.4 Simulation

In urban areas, the vehicle speed is usually between 40 to 60 kilometers per hour. We consider the practical cellular systems that operate at a carrier frequency of 60 GHz with bandwidth of 2 Mb per second. The antennas number at base station is 64 and the number of mobile user is 4. We test our algorithms with two possible channel autocorrelation scenarios, which are vary randomly and monotonically decreasing. A Kalman filter with perfect knowledge of channel autocorrelation is considered as the optimal filter in those cases, and has been used as the benchmark in the simulation.

4.4.1 Random Varying Case

We first consider the case when the channel autocorrelation varies randomly during the tracking period. We adopt the random walk model for the random variation of the channel autocorrelation which have been used in [19]. **Fig. 4.5** shows the performance comparison of different methods. **Figs. 4.6** and **4.7** show the channel tracking process of the best channel. **Figs. 4.8** and **4.9** show the channel tracking process of the worst channel. The ‘best’ and ‘worst’ are referred to small or large average MSE of the channel estimation. The worst case happens when the measure noise is accidentally to be very large.

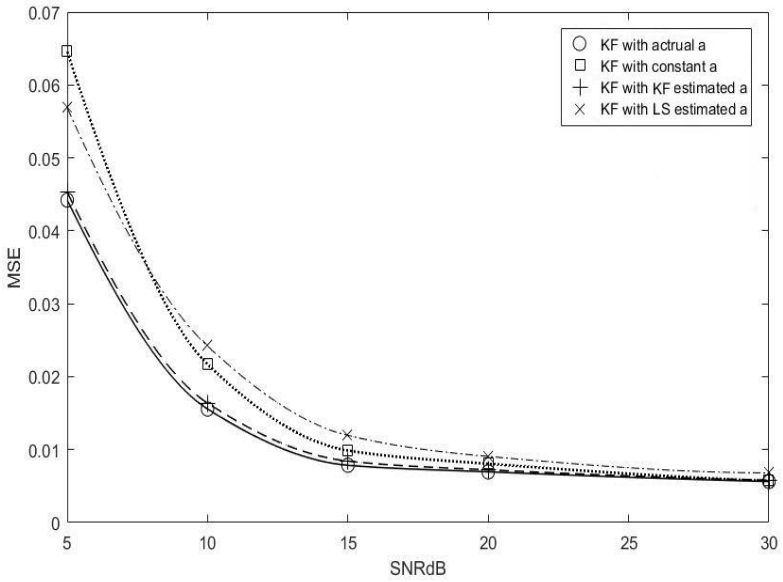

Figure 4.5 Performance of channel coefficients estimation with random varying a.

In **Fig. 4.5,** the 'KF with actual a' is the KF using the actual time varying channel autocorrelation, which is considered to be the optimal KF [18], the 'KF with constant a', or traditional KF, is the KF using the initial autocorrelation through the test the 'KF with LS estimated a' is the method described in **section 4.3.1** and 'KF with KF estimated a' is the method described in **section 4.3.2**. **Fig. 4.5** shows the performance of the second proposed method is very close to the optimal KF.

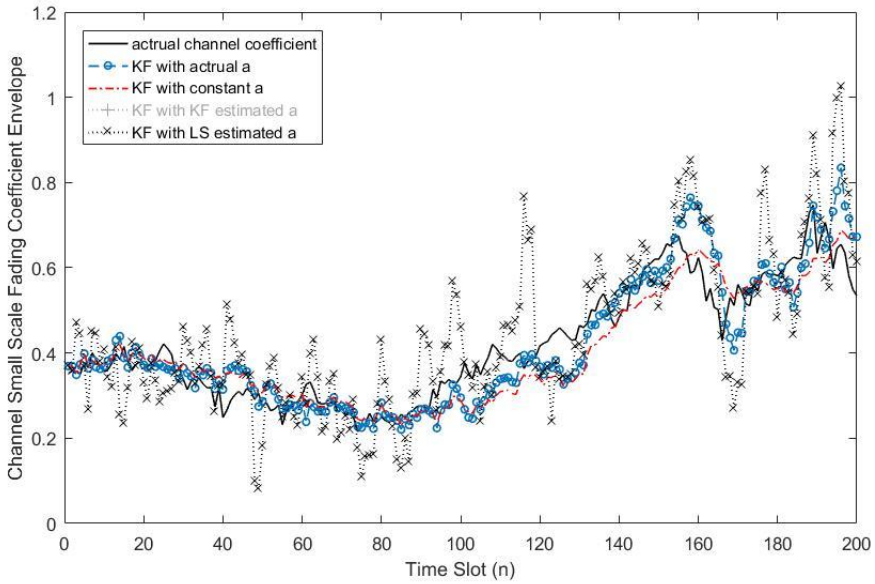

Figure 4.6 Actual and estimated channel variations versus time index n for best-case user at SNR of 10dB with random varying a.

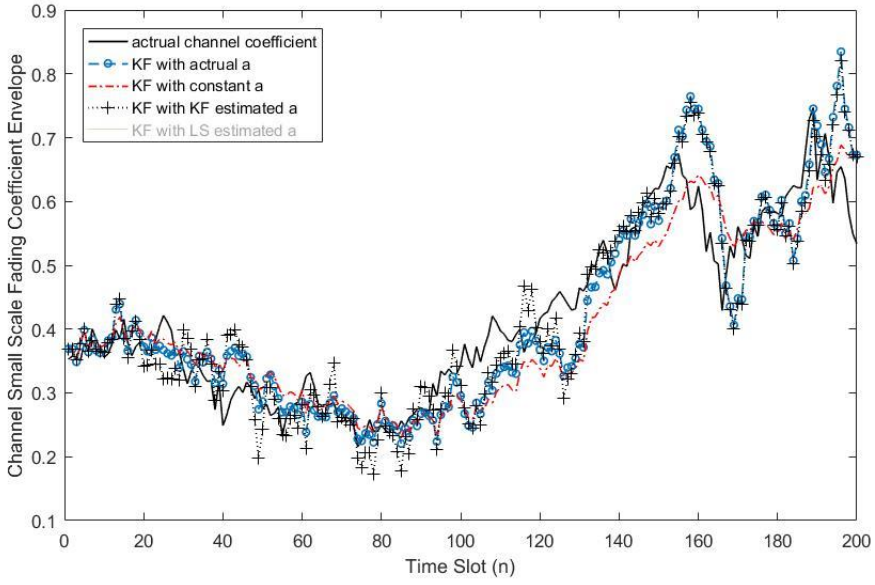

Figure 4.7 Actual and estimated channel variations versus time index n for best-case user at SNR of 10dB with random varying a.

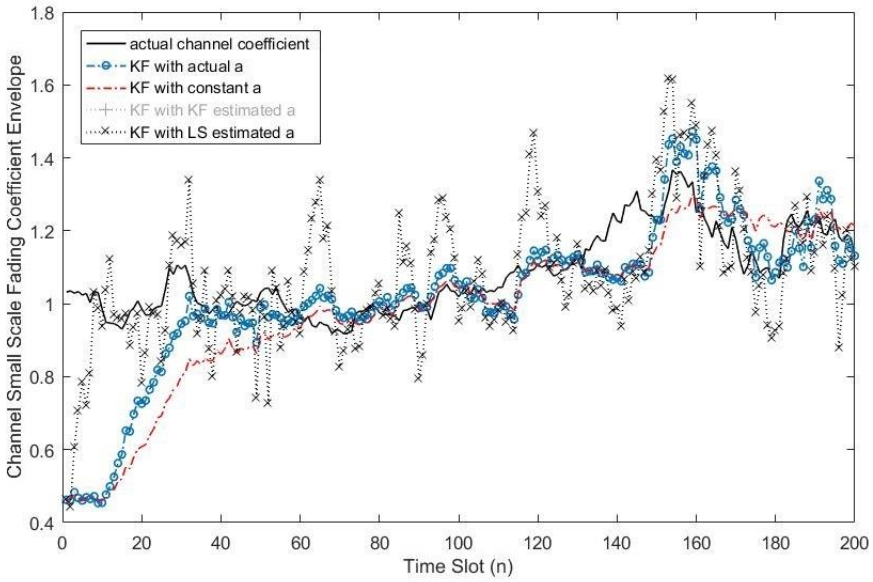

Figure 4.8 Actual and estimated channel variations versus time index n for worst-case user at SNR of 10dB with random varying a.

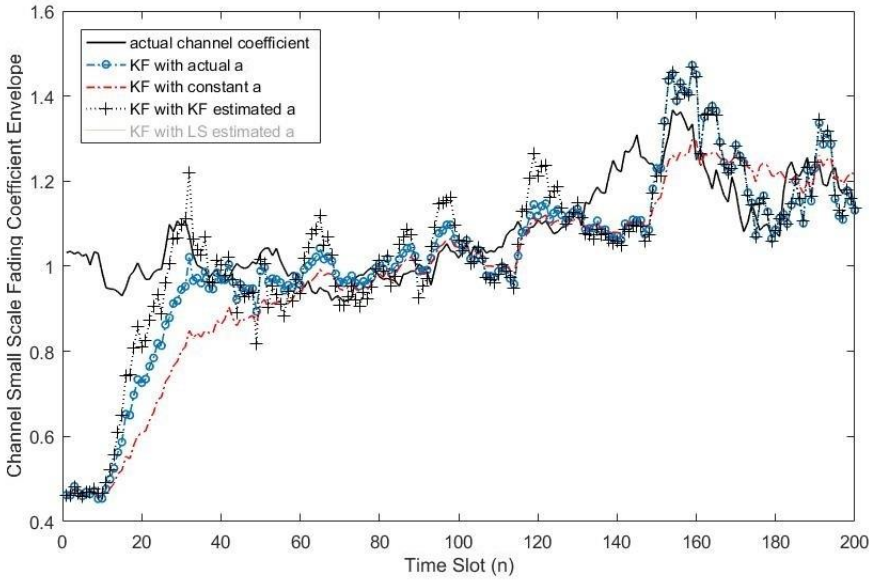

Figure 4.9 Actual and estimated channel variations versus time index n for worst-case user at SNR of 10dB with random varying a.

Figs. 4.7 and **4.9** show the second proposed combined Kalman filters channel autocorrelation and channel coefficients estimator react faster to the variation of channel coefficient than traditional KF and converge to the optimal KF after sufficient number of iterations.

Fig. 4.10 illustrates the random varying channel autocorrelation and its real time estimate from the combined Kalman filters channel autocorrelation and channel coefficients estimator. The performance of channel autocorrelation estimation of LS and KF methods is showed in **Figs. 4.10** and **4.11**, respectively.

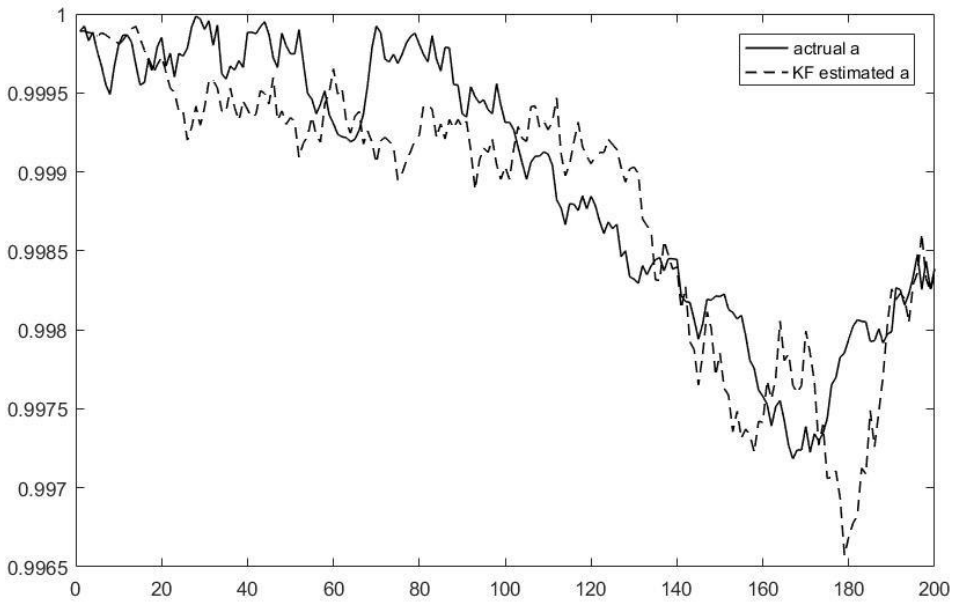

Figure 4.10 Autocorrelation estimation for random a.

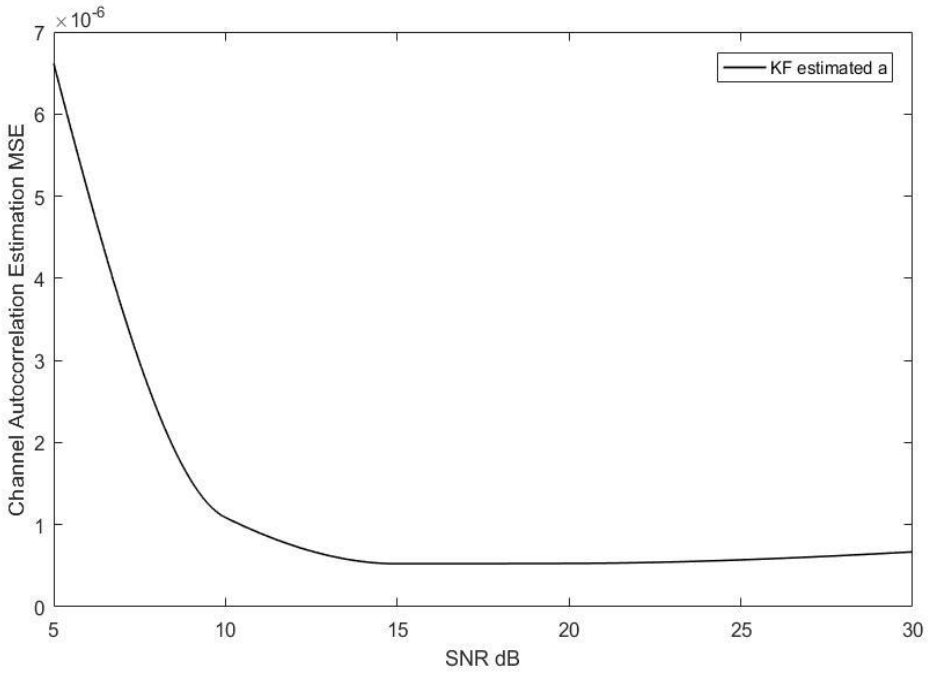

Figure 4.11 Performance of the channel autocorrelation estimator based on KF.

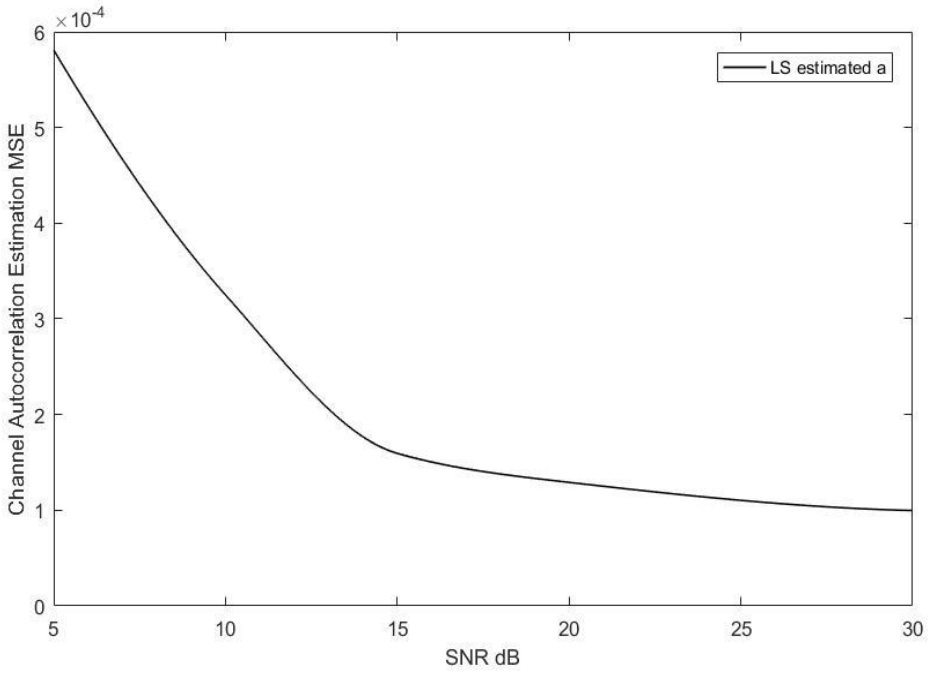

Figure 4.12 Performance of the channel autocorrelation estimator based on LS.

4.4.2 Monotonically Decreasing Case

Second, we consider that the objects in the environment could change momentarily due to the high mobility assumption. The acceleration of the vehicle and suddenly appeared path components could temporally reduce the channel autocorrelation. We set up a random decrease model for the channel autocorrelation variation.

$$a(t+1) = a(t) + \epsilon_a, \tag{4.37}$$

where ϵ_a is a half-normal distributed random variable. **Fig. 4.13** shows the performance comparison of different methods. **Figs. 4.14** and **4.15** show the channel tracking process of the best channel. **Figs. 4.16** and **4.17** show the channel tracking process of the worst channel.

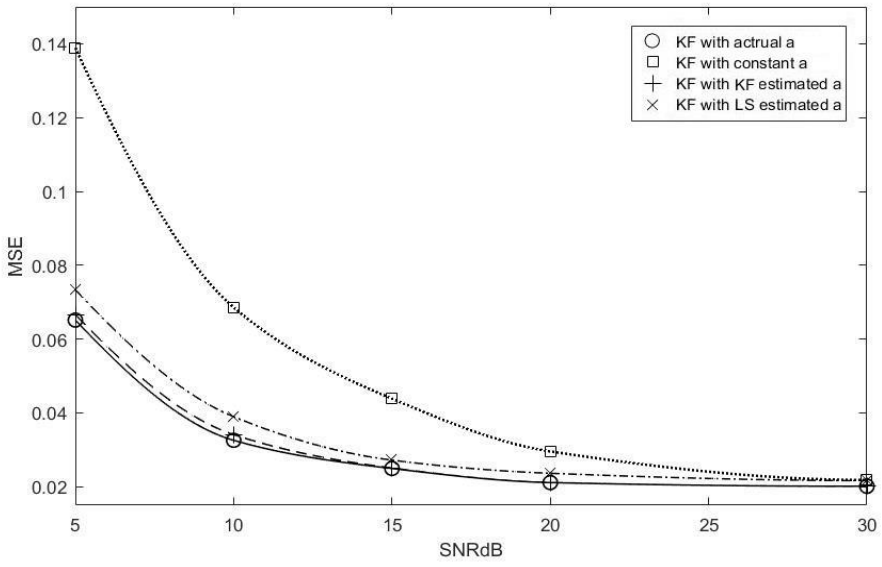

Figure 4.13 Performance of channel coefficients estimation with monotonically decreasing a.

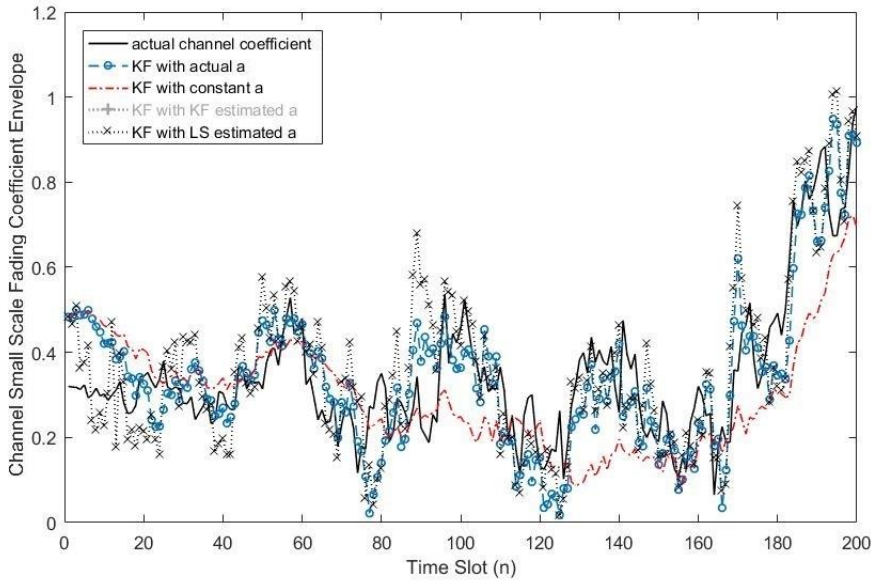

Figure 4.14 Actual and estimated channel variations versus time index n for best-case user at SNR of 10dB with monotonically decreasing a.

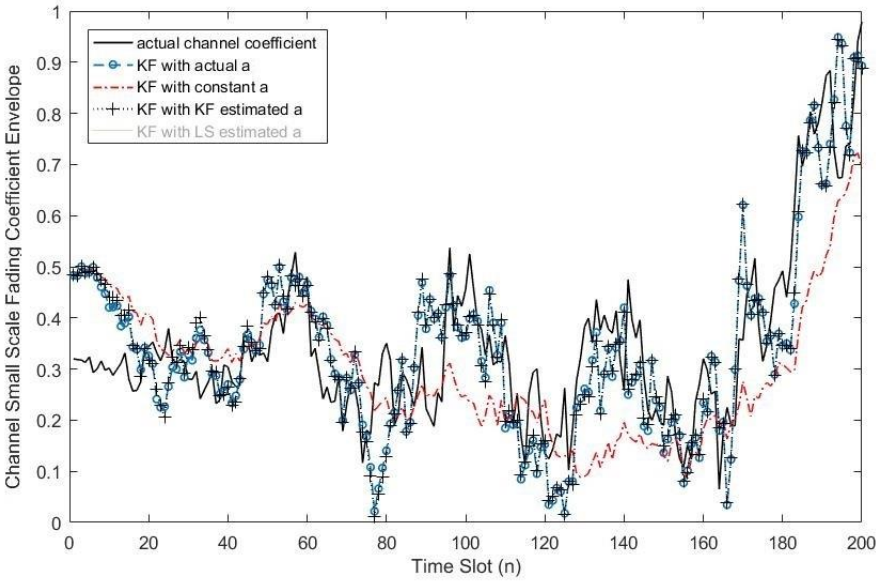

Figure 4.15 Actual and estimated channel variations versus time index n for best-case user at SNR of 10dB with monotonically decreasing a.

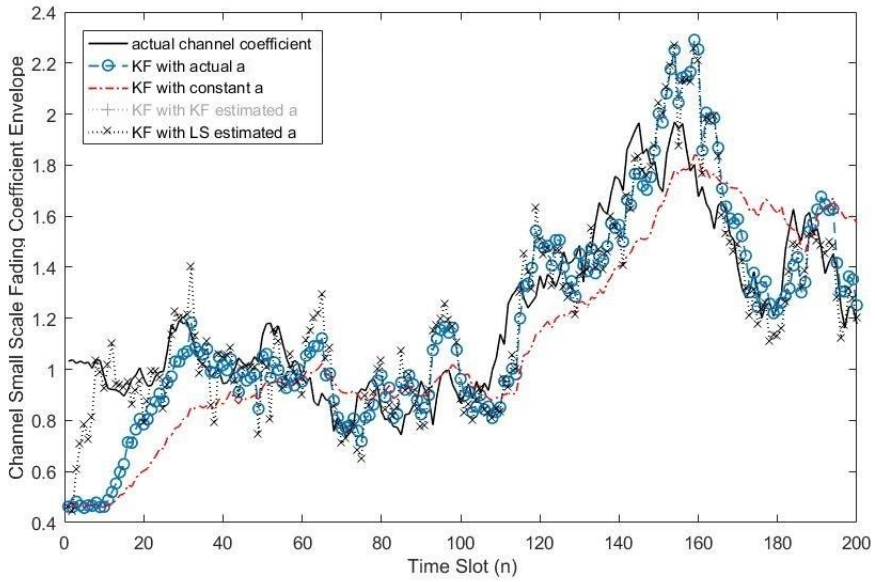

Figure 4.16 Actual and estimated channel variations versus time index n for worst-case user at SNR of 10dB with monotonically decreasing a.

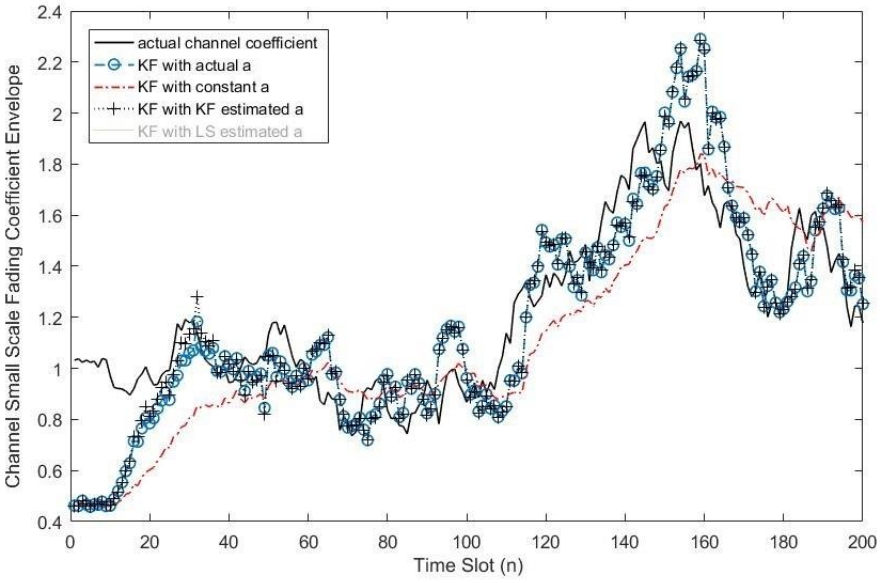

Figure 4.17 Actual and estimated channel variations versus time index n for worst-case user at SNR of 10dB with monotonically decreasing a.

Fig. 4.18 illustrates the monotonically decreasing channel autocorrelation and its real time estimate from the combined Kalman filters channel autocorrelation and channel coefficients estimator. The performance of channel autocorrelation estimation of LS and KF methods is showed in **Figs. 4.19** and **4.20**, respectively.

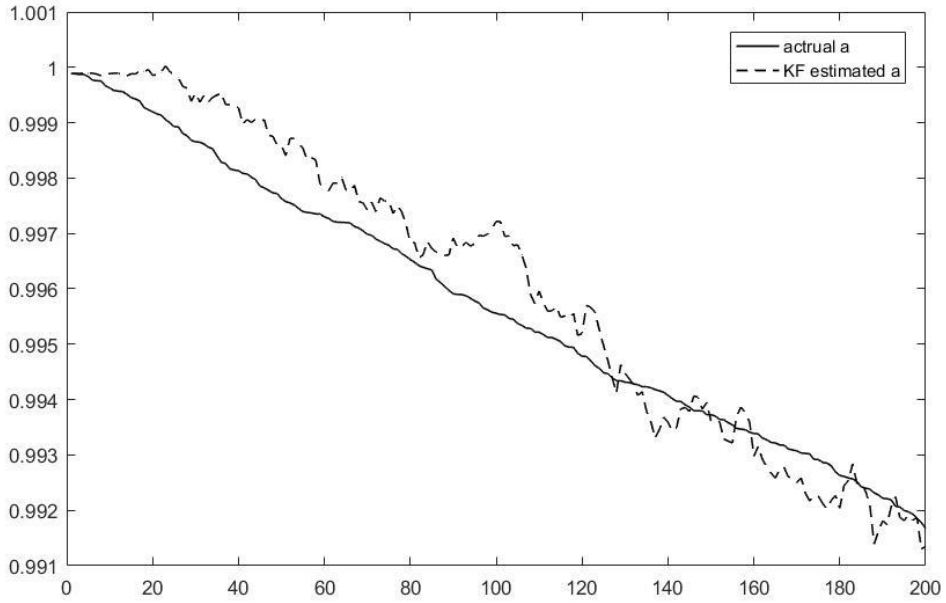

Figure 4.18 Autocorrelation estimation of monotonically decreasing a.

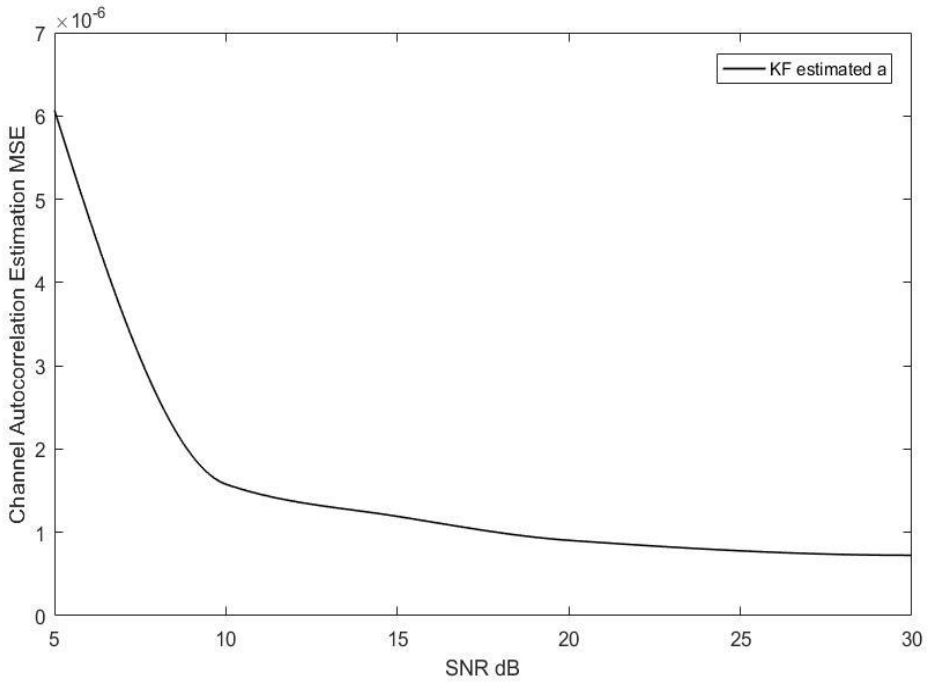

Figure 4.19 Performance of the channel autocorrelation estimator based on KF.

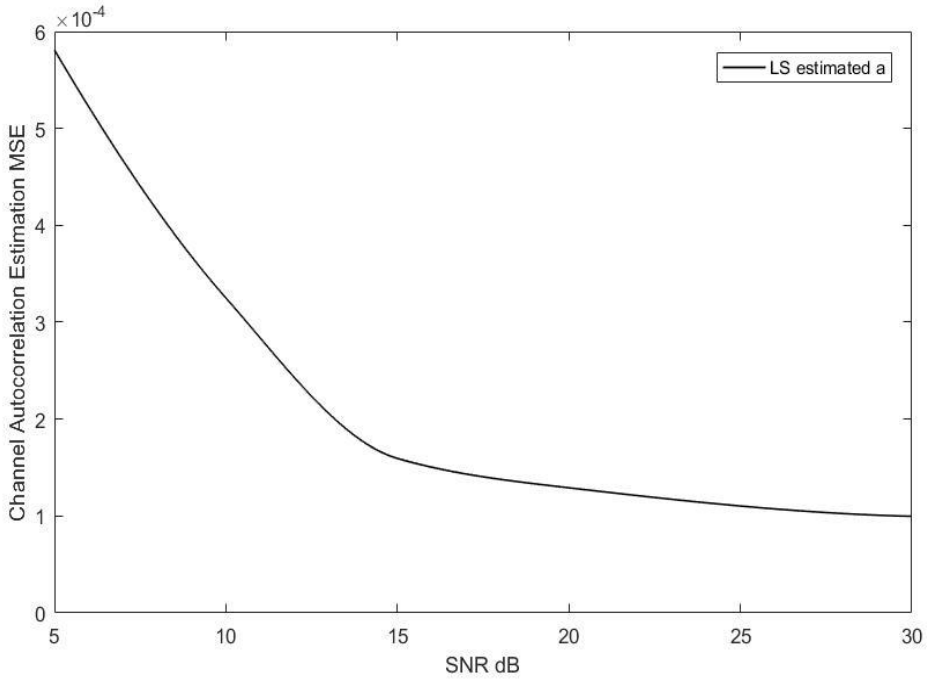

Figure 4.20 Performance of the channel autocorrelation estimator based on LS.

4.4.3 Observations

The **Fig. 4.5** and **4.13** shows the Kalman filter based combined channel coefficient and autocorrelation estimator can improve the performance of the channel estimation in both scenarios. The combined estimator, which uses Kalman filter as channel coefficient estimator and LS as channel autocorrelation estimator, can only provide better result when the channel autocorrelation decreases monotonically. The reason of the different performance of LS and KF channel autocorrelation estimator is due to the accuracy of the LS based channel autocorrelation estimator is not comparable to the Kalman filter based channel autocorrelation, which is showed in **Figs. 4.11, 4.12, 4.19** and **4.20**. However, the computational complexity of the LS method is as low as the traditional Kalman filter, while the computational complexity of the combined KF method is about $\frac{MK+K}{MK}$ times of the traditional method. The performance of Kalman filter based combined channel coefficient and autocorrelation estimator is very close to the performance of the optimal filter, the comparison is showed in **Figs. 4.5** and **4.13**.

5 Applicability Discussion

The most recent existing frame structure for cellular TDD systems is illustrated in **Fig. 5.1** [34]. The system time unit is $T_s = \frac{1}{30720000}$ second which is due to the transceiver sampling time.

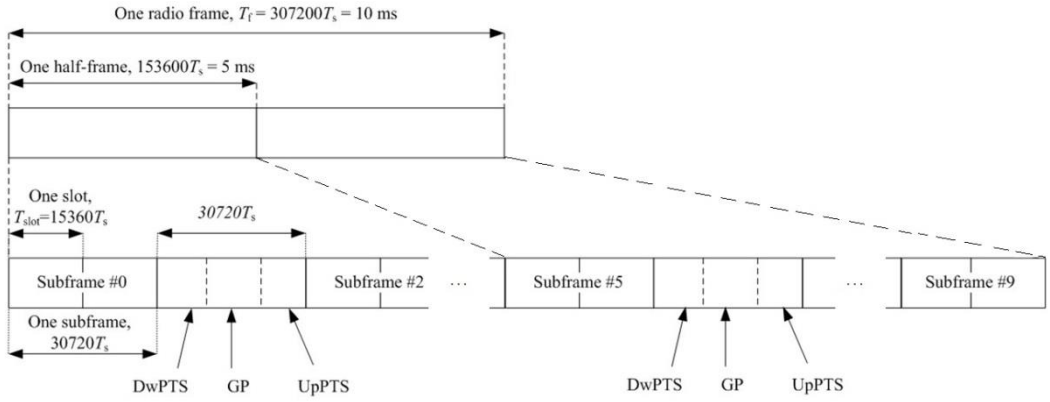

Figure 5.1 Frame Structure of TDD Systems [34]

Each frame is consisted of two half-frames, each half-frame consists of five subframes and each subframe consists of 2 slots. The length of each slot, subframe, half-frame and frame is 0.5ms, 1ms, 5ms and 10ms respectively. **Table 5.1** lists 7 configurations of frame structures. D denotes a downlink subframe and U denotes an uplink subframe. S is the special subframe which is the downlink to uplink switch subframe [34].

Table 1 Uplink-downlink configurations [34]

Uplink-downlink configuration	Downlink-to-Uplink Switch-point periodicity	Subframe number									
		0	1	2	3	4	5	6	7	8	9
0	5 ms	D	S	U	U	U	D	S	U	U	U
1	5 ms	D	S	U	U	D	D	S	U	U	D
2	5 ms	D	S	U	D	D	D	S	U	D	D
3	10 ms	D	S	U	U	U	D	D	D	D	D
4	10 ms	D	S	U	U	D	D	D	D	D	D
5	10 ms	D	S	U	D	D	D	D	D	D	D
6	5 ms	D	S	U	U	U	D	S	U	U	D

Based on **Table 5.1**, the time interval between two reference signals is varying from 1ms to 10ms due to the fact that reference signals are only assigned at uplink subframes.

In certain situations, the channel coherence time will be much shorter than the intervals between two reference signals. For such cases, the proposed combined Kalman filter channel autocorrelation and coefficients estimator will enhance the systems' robustness. The data symbol is picked every 0.01ms to perform the channel autocorrelation and coefficients estimation. This process can be done at either base station side or mobile user side that benefit from its low computational complexity. **Fig. 5.2** illustrates the data selection structure for channel autocorrelation and coefficients estimation. The blue data symbols denote the data symbols which are picked for estimation.

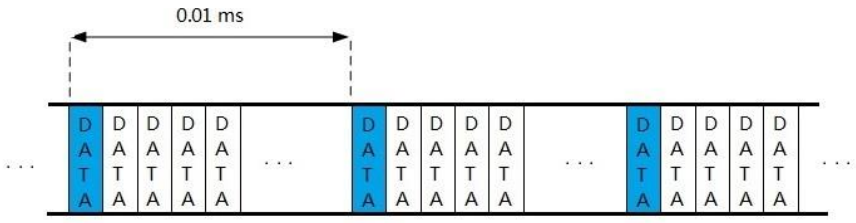

Figure 5.2 Select data for channel autocorrelation and coefficients estimation.

6 Conclusion

A new and effective channel estimation method for massive multi-user MIMO uplink systems based on the Kalman filter is proposed in this thesis. We consider an urban mobile communication scenario with high mobility such that it causes a relatively rapid channel autocorrelation variation. The channel is assumed to be a Rayleigh fading channel which is frequency nonselective and time varying. The substantially increased carrier frequency in 5G cellular systems results in a much larger Doppler spread and causes faster channel variations. The base stations also suffer from ICI induced from neighboring cells that use the same reference pilot sequences (pilot contamination).

A first order Gaussian Markov model is adopted to represent the channel dynamics. By using the data detected with predicted channel coefficient matrix as the measurement matrix, we cast the channel estimator into Kalman filter form. By exploring the substantially increased receiver diversity due to the massive receiver antennas, we found a way to estimate the channel autocorrelation efficiently, which further allows us to formulate a channel autocorrelation estimator. The Kalman filter minimizes the effect of the Gaussian noise, which occurs in the channel dynamics and the receiver devices. The ICI is assumed to be a Gaussian process and thus its effect can be minimized by a Kalman filter. The autocorrelation estimator helps the channel coefficient estimator performs with good robustness to the variation of channel autocorrelation. Then the combined channel coefficient and autocorrelation estimator can perform almost optimally in a time-varying channel

autocorrelation environment.

In 5G TDD cellular systems operating in the TDD mode, the channel estimation is performed at the base station. Thus, the reference pilot signals are assigned to the uplink streams. Such systems cannot perform well if the channel coefficient changes between two reference pilot sequences. The proposed method can prolong the time between two reference pilot sequences without compromising system performance and helps both uplink and downlink configurations work properly in high mobility scenario.

7 Bibliography

[1] "Lecture Notes Principles of Digital Communications I Electrical Engineering and Computer Science, MIT OpenCourseWare", Ocw.mit.edu, 2016. [Online]. Available: http://ocw.mit.edu/courses/electrical-engineering-and-computer-science/6-450-principles-of-digital-communications-i-fall-2006/lecture-notes. [Accessed: 05- Sep- 2016].

[2] Nokia White Paper, "5G Use Cases and Requirements", alcatel-lucent.com, 2016. [Online]. Available: http://resources.alcatel-lucent.com/asset/200010. [Accessed: 05- Sep- 2016].

[3] L. Lu, G. Y. Li, A. L. Swindlehurst, A. Ashikhmin and R. Zhang, "An Overview of Massive MIMO: Benefits and Challenges," *IEEE Signal Processing*, vol. 8, no. 5, pp. 742-758, Oct. 2014.

[4] E. G. Larsson, O. Edfors, F. Tufvesson and T. L. Marzetta, "Massive MIMO for next generation wireless systems," *IEEE Communications Magazine*, vol. 52, no. 2, pp. 186-195, February 2014.

[5] E. Björnson, E. G. Larsson, and T. L. Marzetta, "Massive MIMO: Ten myths and one critical question," IEEE Communications Magazine, vol. 54, no. 2, pp. 114–123, Feb. 2016.

[6] T. L.Marzetta, "Noncooperative cellular wireless with unlimited numbers of base station antennas, " *IEEE Trans. Wireless Commun.*, vol. 9, no. 11, pp. 3590–3600, Nov. 2010.

[7] O. Elijah, C. Y. Leow, T. A. Rahman, S. Nunoo and S. Z. Iliya, "A Comprehensive Survey of Pilot Contamination in Massive MIMO—5G System," *IEEE Communications Surveys & Tutorials*, vol. 18, no. 2, pp. 905-923, 2016.

[8] M. Masood, L. H. Afify and T. Y. Al-Naffouri, "Efficient Coordinated Recovery of Sparse Channels in Massive MIMO," *IEEE Transactions on Signal Processing*, vol. 63, no. 1, pp. 104-118, Jan.1, 2015.

[9] M. Masood, L. H. Afify and T. Y. Al-Naffouri, "Efficient collaborative sparse channel estimation in massive MIMO," *2015 IEEE International Conference on Acoustics, Speech and Signal Processing (ICASSP)*, pp.

2924-2928, South Brisbane, 2015.

[10] M. S. Sim, J. Park, C. B. Chae and R. W. Heath, "Compressed channel feedback for correlated massive MIMO systems," *Journal of Communications and Networks*, vol. 18, no. 1, pp. 95-104, Feb. 2016.

[11] X. Rao, V. K. N. Lau and X. Kong, "CSIT estimation and feedback for FDD multi-user massive MIMO systems," *2014 IEEE International Conference on Acoustics, Speech and Signal Processing (ICASSP)*, pp. 3157-3161, Florence, 2014.

[12] X. Rao and V. K. N. Lau, "Compressive Sensing With Prior Support Quality Information and Application to Massive MIMO Channel Estimation With Temporal Correlation," *IEEE Transactions on Signal Processing*, vol. 63, no. 18, pp. 4914-4924, Sep.15, 2015.

[13] Z. Chen and C. Yang, "Pilot Decontamination in Wideband Massive MIMO Systems by Exploiting Channel Sparsity," *IEEE Transactions on Wireless Communications*, vol. 15, no. 7, pp. 5087-5100, Jul. 2016.

[14] L. You, X. Gao, A. L. Swindlehurst and W. Zhong, "Adjustable phase shift pilots for sparse massive MIMO-OFDM channels," *2015 IEEE 16th International Workshop on Signal Processing Advances in Wireless Communications (SPAWC)*, pp. 206-210, Stockholm, 2015.

[15] Kalman, R. E. 1960. "A New Approach to Linear Filtering and Prediction Problems," *Transaction of the ASME—Journal of Basic Engineering*, pp. 35-45, Mar. 1960.

[16] I. Sheikh, Noor Khan and P. Rapajic, "Kalman filter based channel estimation in OFDM multi-user single-input-multi-output system," *Spread Spectrum Techniques and Applications, 2004 IEEE Eighth International Symposium on*, pp. 802-806, 2004.

[17] B. Karakaya, "An adaptive channel interpolator based on Kalman filter for LTE uplink in high Doppler spread environments," *EURASIP J. Wirel. Commun. Netw*, pp. 1–10, 2009.

[18] Ki-Young Han, Sang-Wook Lee, Jun-Seok Lim and Koeng-Mo Sung, "Channel estimation for OFDM with fast fading channels by modified Kalman filter," *IEEE Transactions on Consumer Electronics*, vol. 50, no. 2, pp. 443-449, May 2004.

[19] X. Dai, W. Zhang, J. Xu, J. E. Mitchell, and Y. Yang, "Kalman interpolation filter for channel estimation of LTE downlink in high-mobility environments, " *EURASIP J. Wireless Commun. Networks*, vol. 2012:232, Jul. 2012.

[20] M. Huang, X. Chen, L. Xiao, S. Zhou, and J. Wang, "Kalman-filter-based channel estimation for orthogonal frequency-division multiplexing systems in time-varying channels," IET Communications, vol. 1, no. 4, p. 795, 2007.

[21] W. C. Jakes, Ed., Microwave mobile communications. United States: IEEE Publications,U.S., 1994.

[22] "5gamericas: FACT SHEET: SPECTRUM FRONTIERS RULES IDENTIFY, OPEN UP VAST AMOUNTS OF NEW HIGH-BAND SPECTRUM FOR NEXT GENERATION (5G) WIRELESS BROADBAND", 4gamericas.org, 2016. [Online]. Available: http://www.4gamericas.org/en/newsroom/industry-news/fact-sheet-spectrum-frontiers-rules-identify-open-vast-amounts-new-high-band-spectrum-next-generation-5g-wireless-broadband/. [Accessed: 05- Sep- 2016].

[23] A. Goldsmith, "Wireless Communications," *Cambridge University Press*, Cambridge, 2005.

[24] V. H. McDonald, "The Cellular Concept," *Bell System Tech. J*, pp. 15-49, Jan. 1979.

[25] M. C. Jeruchim , "Simulation Of Communication Systems (2Nd Ed)," *Plenum*, p547, New York, 1992.

[26] R. H. Clarke, "A Statistical Theory of Mobile-Radio Reception," *Bell System Technical Journal*, vol. 47, no. 6, pp. 957-1000, 1968.

[27] D. Tse, "Fundamentals of Wireless Communication," *Cambridge University Press*, Cambridge, 2005.

[28] L. Zheng, Tse, "Diversity and Multiplexing: A Fundamental Tradeoff in Multiple-antenna Channels." *Information Theory, IEEE Transactions*, vol. 49, no. 5, pp. 1073-096, 2003.

[29] F. Rusek, D. Persson, B. K. Lau, E. G. Larsson, T. L. Marzetta, and F. Tufvesson, "Scaling up MIMO: Opportunities and challenges with very large arrays," IEEE Signal Processing Magazine, vol. 30, no. 1, pp. 40–60, Jan. 2013.

[30] G. Calcev *et al*., "A Wideband Spatial Channel Model for System-Wide Simulations," *IEEE Transactions on Vehicular Technology*, vol. 56, no. 2, pp. 389-403, March 2007.

[31] K. Baddour, N. Beaulieu, "Autoregressive modeling for fading channel simulation," *IEEE Trans. Wireless Communications*, vol. 4, no. 4, pp. 1650-1662. 2005.

[32] L. Tong, Sadler and M. Dong, "Pilot-assisted wireless transmissions: General model, design criteria, and signal processing," *IEEE Signal Processing Magazine*, vol. 21, no. 6, pp. 12-25, 2004.

[33] S. Noh, Zoltowski, Y. Sung and Love, "Pilot Beam Pattern Design for Channel Estimation in Massive MIMO Systems," *IEEE Signal Processing*, vol. 8, no. 5, pp. 787-801, 2014.

[34] 3GPP, "TS 36.211 V13.2.0 Physical Channels and Modulation," Jun. 2016